AD 258 750

UNIVERSITY OF

MARYLAND

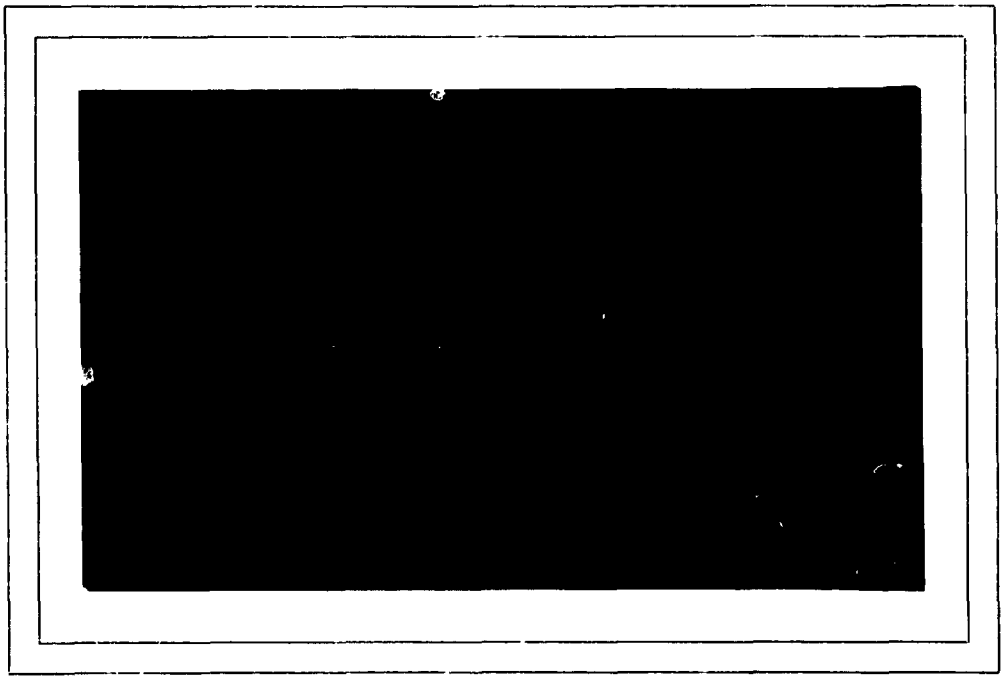

NOX

THE INSTITUTE FOR FLUID DYNAMICS

and

APPLIED MATHEMATICS

AFOSR-765

Technical Note BN-247 May, 1961
AFOSR-765

STABILITY AND TRANSITION OF THE FREE-CONVECTION LAYER ALONG A VERTICAL FLAT PLATE*

by

Albin A. Szewczyk

University of Maryland
College Park, Maryland

* This research was supported in part by the U. S. Air Force under Contract #AF 49(638)645 monitored by the Air Force Office of Scientific Research of the Air Research and Development Command.

Bibliographical Control Sheet

1. (Originating agency and/or monitoring agency)

   O.A.: University of Maryland, College Park, Maryland

   M.A.: Mechanics Division, Air Force Office of Scientific Research

2. (Originating agency and/or monitoring agency report number)

   O.A.: Technical Note BN-247

   M.A.: AFOSR- 765

3. Title and classification of title:

   STABILITY AND TRANSITION OF THE FREE-CONVECTION LAYER ALONG A VERTICAL FLAT PLATE

4. Personal author (s): Albin A. Szewczyk

5. Date of report: May, 1961

6. Pages: 82

7. Illustrative material: 29

8. Prepared for Contract No. (s): AF 49(638)645

9. Prepared for Project Code (s): and/or No. (s): 9781

10. Security classification: Unclassified

11. Distribution limitations: None

12. Abstract: The free-convection layer along a vertical flat plate is investigated theoretically as well as experimentally with a view to studying its instability and "natural" transition from laminar to turbulent flow. Stability calculations are carried out based upon the small perturbation theory for the exact velocity profile for the Prandtl number 10.

Temperature profiles are measured along a vertical electrically-heated brass plate. By the use of a dye technique the natural transition mechanism is investigated, i.e., discrete vortex lines and their subsequent distortion into three-dimensional pattern and eventual breakdown is carefully studied.

In addition a double-row vortex system, which arises in the free-convection layer, is investigated. Its mechanics and overall effect on the stability and transition of the free-convection layer are discussed.

ACKNOWLEDGMENTS

The author would like to take this opportunity to express his sincere appreciation to Dr. Francis R. Hama for his guidance and helpful advice furnished during the course of this investigation.

To Dr. Shan-Fu Shen sincere thanks for his valuable advice and discussions afforded the author in regard to the theoretical aspects of the stability problem.

To Professor Charles A. Shreeve sincere thanks for his encouragement and helpful discussions during this investigation.

Last but not least profound thanks to all those who in some way helped to complete this dissertation.

In addition I gratefully acknowledge the support of the United States Air Force Office of Scientific Research under Contract No. AF 49(638)645 which made this research possible.

Nomenclature

A_n, B_n	arbitrary constants
c	wave propagation speed
c_p	specific heat at constant pressure
Fr	Froude number
f	dimensionless stream function
f'	dimensionless velocity
g	gravitational constant
G	modified Grashof-number parameter based on x
Gr	Grashof number based on x
K_i, K_o	constants
k	coefficient of heat conductivity
p	total pressure
P	pressure of the basic flow
Pr	Prandtl number
Ra	Rayleigh number
t'	temperature perturbation function
t	absolute temperature

t	ambient temperature
t_w	wall temperature
z	dimensionless independent variable
u	velocity parallel to surface
U	velocity of basic flow
v	velocity normal to surface
x	distance from leading edge of the plate
y	normal distance from surface
α	wave number
β	coefficient of volumetric expansion
δ	boundary-layer thickness
ϵ	small parameter
η	dimensionless similarity variable
θ	dimensionless disturbance temperature function
ϑ	dimensionless temperature function
λ	wave length of disturbance wave
μ	viscosity
ν	kinematic viscosity

ξ	dimensionless temperature amplitude function
ρ	density
τ	time
ϕ	dimensionless velocity amplitude function
ψ	stream function
$\sim$	disturbance quantity
$(\overline{\ })$	dimensional quantity

Subscripts

i	refers to inner critical layer
o	refers to outer critical layer
0, w	evaluated at the wall,

Introduction

Transition from laminar to turbulent flow has drawn the attention of many investigators throughout the years. In most of the experimental as well as the theoretical studies over-all effects of certain imposing conditions on transition have been found. Many details of the actual mechanism of transition, however, still remain unknown. In recent years investigations have been centered on clarifying the intricate mechanism of transition through experimental studies.

Experimental studies have been greatly supplemented by the development of small-disturbance stability theory. Although the stability theory provides no insight into the actual mechanism of transition, it does determine under what conditions certain small disturbances would amplify or decay in a given flow. Schubauer and Skramstad [1] [1] confirmed the theory of small distrubances by performing wind-tunnel experiments. They introduced small disturbances artificially in the flow by means of a vibrating ribbon situated on a flat plate. The small wave disturbances are observed to be amplified as the flow progresses downstream under the conditions as properly predicted by the theory. The wave intensifies its strength as it is amplified until a turbulent spot is produced. The turbulent spot growing in size envelops the adjacent portions of laminar flow. The growth of a turbulent spot has been studied in detail by Schubauer and Klebanoff [2] . By the use of a hot-wire anemometer Klebanoff and Tidtrom [3] (see also Schubauer [4]) investigated the highly

---

1 Numbers in brackets designate References at end of paper.

three-dimensional features involved in the transition process.

Hama, Long and Hegarty [5] explained some significant features of the transition mechanism through the flow-visualization technique by means of dye injection. Dye patterns of two-dimensional discrete vortices shed by a trip wire on a flat plate towed in a water tank were observed. Observations disclosed that the initially two-dimensional discrete vortices deformed into three-dimensional vortex loops. As the vortex loops moved downstream they were stretched and deformed further until a turbulent spot appeared near the head of the loop. This spot then gave rise to highly turbulent motion. Hama [6] recently has performed similar experiments in the water tank but used a vibrating ribbon as the stimulating device in place of the trip wire used previously. He concluded from these experiments that the formation of a vortex loop was an essential feature in the transition process.

In the above mentioned experiments some kind of stimulating device was always used to provoke the onset of turbulence. Several experiments dealing with the phenomena of "natural transition", i.e., without the aid of artificial stimulation have been performed. Fales [7] . Hama [8] , and Hegarty [9] concerned themselves with the stability and transition of flow over a flat plate stopped suddenly. Hama [10] , [11] , also considered the transition process behind a backward-facing step and in the wake behind a circular cylinder, respectively.

In order to attain a better basic understanding of the "natural transition" process in contrast to the artificially-stimulated transition process the present investigation was initiated. The free-convection layer along a vertical flat plate is inherently unstable because of the particular velocity profile in it and, therefore, affords an excellent opportunity of studying its instability and the phenomena associated with "natural transition".

Eckert and Soehnghen [12] investigated the transition process in the free-convection layer along a heated vertical flat plate in air. The interferograms, however, restricted the observations to only a two-dimensional picture. Since the transition process is intrinsically three-dimensional, only a limited understanding of the transition process was obtained.

A similar work was reported by Birch [13] who introduced a controlled disturbance into the flow about an isothermal wall. He attempted to determine the properties of a critical or natural frequency that would produce incipient instability. An empirical relation between the frequency and Rayleigh number was determined. Gartrell [14] made a further study into the effect of forced oscillations of the free-convection layer. He found that the empirical relation developed by Birch applied only to the specific test conditions of his study and not generally to free-convection flows. In addition Gartrell could find no apparent relation among the various flow-parameters which could be used to predict the effect of variations in flow conditions and disturbances

on flows of this type. Thus, the effect of induced disturbances on a flow, which was known to be highly unstable without artificial disturbances still remains open.

Other experiments on transition in the free-convection fields over vertical flat plates and cylinders were performed by Saunders [15], [16], Hermann [17], Fujii [18], and Larson [19]. These authors, however, were essentially concerned with the transition Rayleigh number. They found that transition took place at the Rayleigh number approximately 2 to 4 x 10^9 in various fluids.

Lack of theoretical investigations into the instability of free-convection flow provided an additional reason for careful analysis of the problem. Although Plapp [20] performed an analysis on a polynomial approximation of the free-convection velocity profile in air, it was desired in the present investigation to obtain a more accurate solution based upon the exact velocity profile. Since the experiments were to be performed in water, a velocity profile for larger Prandtl numbers needed to be considered.

Theoretical Analysis

Consider a steady free-convection flow about a vertical heated plate. The basic (conservation) equations governing this motion under the boundary-layer approximations are:

$$\frac{\partial u}{\partial x} + \frac{\partial v}{\partial y} = 0 \,, \tag{1}$$

$$u \frac{\partial u}{\partial x} + v \frac{\partial u}{\partial y} = \nu \frac{\partial^2 u}{\partial y^2} + g\beta(t - t_\infty) \,, \tag{2}$$

$$u \frac{\partial t}{\partial x} + v \frac{\partial t}{\partial y} = \frac{k}{\rho c_p} \frac{\partial^2 t}{\partial y^2} \,. \tag{3}$$

where u and v are the velocity components in x- and y- directions, respectively, g the gravitational constant, β the coefficient of thermal expansion, t and t_∞ the temperature of the fluid at any location and the temperature of the ambient fluid, respectively, and $k/\rho c_p$ the thermal diffusivity. Physical configuration and co-ordinate system are shown in the following sketch.

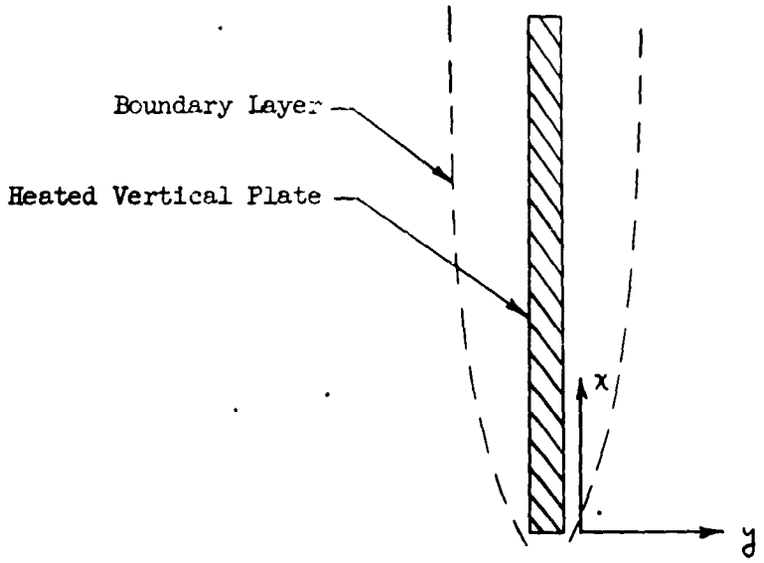

When a stream function ψ is defined such that $u = \partial\psi/\partial y$ and $v = -\partial\psi/\partial x$ the continuity equation is satisfied. E. Pohlhausen [21] showed that, by the use of a similarity transformation

$$\eta = \left[\frac{g\beta(t_w - t_\infty)}{4\nu_\infty^2 x}\right]^{\frac{1}{4}} y = \left(\frac{Gr_x}{4}\right)^{\frac{1}{4}} \frac{y}{x} , \tag{4}$$

$$\psi = 4\nu_\infty x^{\frac{3}{4}} \left[\frac{g\beta(t_w - t_\infty)}{4\nu_\infty^2}\right]^{\frac{1}{4}} f(\eta) , \tag{5}$$

and a dimensionless local temperature $\theta(\eta) = (t - t_\infty)/(t_w - t_\infty)$, the basic equations can be reduced to a set of ordinary differential equations

$$f''' + 3ff'' - 2f'^2 + \theta = 0 , \tag{6}$$

$$\theta'' + 3Pr f\theta = 0 , \tag{7}$$

where primes indicate the derivatives with respect to η . The boundary conditions are

$$f(0) = f'(0) = 0 , \qquad \theta(0) = 1 ,$$

$$f'(\infty) = \theta(\infty) = 0 . \tag{8}$$

This set of equations have been solved by E. Pohlhausen, and its solution is extended by Schuh [22] to the case of large Prandtl

numbers. Ostrach [23] performed a more accurate calculation of this system of equations for the Prandtl numbers 0.01, 0.72, 1.0, 2, 10, 100, 1000, on an electronic computer. The numerical results obtained by Ostrach are tabulated in NACA TN 2635 and exclusively used in the ensuing computational and experimental work.

The stability of the basic free-convection flow will be examined by the method of small perturbations, i.e., we inquire whether a certain disturbance, which is superposed to the basic flow and which satisfies the equations of motion, is amplified or damped out. A fundamental assumption of the hydrodynamic stability theory is the "parallel-flow" condition which stipulates that the mean velocity U depends upon y only. The boundary-layer flow approximates the parallel-flow concept very well because the variation of u with respect to the x -co-ordinate is much smaller than that with respect to y . In addition, we need only to consider two-dimensional disturbances in regard to the instability criterion, since H. B. Squire's theorem [24] states that a two-dimensional flow is more unstable for two-dimensional disturbances than for three-dimensional disturbances.

The basic flow described by $U = U(y)$, $V = 0$, $P(x,y)$, $T(x,y)$ is assumed to be a solution of the steady-state equations. Upon this basic flow we superimpose a two-dimensional disturbance varying in time and space. When the disturbance velocity components, pressure, and temperature are denoted by $\tilde{u}(x,y,\tau)$, $\tilde{v}(x,y,\tau)$, $\tilde{p}(x,y,\tau)$, $\tilde{t}(x,y,\tau)$, the resulting motion is given by

$$u = U + \tilde{u} \; ; \quad v = \tilde{v} \; ; \quad p = P + \tilde{p} \; ; \quad t = T + \tilde{t} \; .$$

These quantities are substituted into the two-dimensional equation of continuity, the incompressible Navier-Stokes equations and the energy equation, as given by

$$\frac{\partial u}{\partial x} + \frac{\partial v}{\partial y} = 0 \ , \tag{9}$$

$$\frac{\partial u}{\partial \tau} + u\frac{\partial u}{\partial x} + v\frac{\partial u}{\partial y} = -\frac{\partial p}{\partial x} + \nu \nabla^2 u + g\beta(t - t_\infty) , \tag{10}$$

$$\frac{\partial v}{\partial \tau} + u\frac{\partial v}{\partial x} + v\frac{\partial v}{\partial y} = -\frac{\partial p}{\partial y} + \nu \nabla^2 v , \tag{11}$$

$$\frac{\partial t}{\partial \tau} + u\frac{\partial t}{\partial x} + v\frac{\partial t}{\partial y} = \frac{k}{\rho c_p} \nabla^2 t , \tag{12}$$

where $\nabla^2 = \frac{\partial^2}{\partial x^2} + \frac{\partial^2}{\partial y^2}$. After dropping the basic flow quantities, which are already assumed to satisfy the conservation equations, and neglecting the quadratic terms in the disturbance quantities, these equations reduce to

$$\frac{\partial \tilde{u}}{\partial x} + \frac{\partial \tilde{v}}{\partial y} = 0 \ , \tag{13}$$

$$\frac{\partial \tilde{u}}{\partial \tau} + U\frac{\partial \tilde{u}}{\partial x} + \tilde{v}\frac{dU}{dy} = -\frac{1}{\rho}\frac{\partial \tilde{p}}{\partial x} + \nu \nabla^2 \tilde{u} + g\beta \tilde{t} , \tag{14}$$

$$\frac{\partial \tilde{v}}{\partial \tau} + U\frac{\partial \tilde{v}}{\partial x} = -\frac{1}{\rho}\frac{\partial \tilde{p}}{\partial y} + \nu \nabla^2 \tilde{v} , \tag{15}$$

$$\frac{\partial t}{\partial \tau} + U\frac{\partial \tilde{t}}{\partial x} + \tilde{v}\frac{dT}{dy} = \frac{k}{\rho c_p} \nabla^2 \tilde{t} . \tag{16}$$

By cross-differentiating equations (14) and (15), the pressure terms are eliminated, and this system of equations reduces to the following equations:

$$\frac{\partial \tilde{u}}{\partial x} + \frac{\partial \tilde{v}}{\partial y} = 0 \quad , \tag{17}$$

$$\frac{\partial^2 \tilde{u}}{\partial y\, \partial \tau} - \frac{\partial^2 \tilde{v}}{\partial x\, \partial \tau} + U\left[\frac{\partial^2 \tilde{u}}{\partial x\, \partial y} - \frac{\partial^2 \tilde{v}}{\partial x^2}\right] + \frac{dU}{dy}\left[\frac{\partial \tilde{u}}{\partial x} + \frac{\partial \tilde{v}}{\partial y}\right]$$

$$+ \tilde{v}\,\frac{d^2 U}{dy^2} = \nu\left[\frac{\partial}{\partial y}\left(\nabla^2 \tilde{u}\right) - \frac{\partial}{\partial x}\left(\nabla^2 \tilde{v}\right)\right] + g\beta\,\frac{\partial \tilde{t}}{\partial y} \quad , \tag{18}$$

$$\frac{\partial \tilde{t}}{\partial \tau} + U\,\frac{\partial \tilde{t}}{\partial x} + \tilde{v}\,\frac{dT}{dy} = \frac{k}{\rho c_p}\,\nabla^2 \tilde{t} \quad . \tag{19}$$

Since we have already assumed that the perturbation is two-dimensional, any Fourier component of arbitrary two-dimensional oscillations may have (x, τ) dependence in the form $e^{i\bar{\alpha}(x - \bar{c}\tau)}$. In this expression, $\bar{\alpha} = 2\pi/\lambda$ is real and positive and represents the wave number of the disturbance. On the other hand, $\bar{c}$ is complex, $\bar{c} = \bar{c}_r + i\,\bar{c}_i$, in which $\bar{c}_r$ denotes the propagation velocity of the wave disturbance in the x-direction and $\bar{c}_i$ denotes the amplification factor. Depending upon whether $\bar{c}_i$ is positive, zero or negative, the wave is amplified, neutral or damped out. The continuity equation for the perturbed velocity is satisfied by introducing a perturbation stream function of the form

$$\tilde{\Psi}(x,y,\tau) = \bar{\phi}(y)\, e^{i\bar{\alpha}(x-\bar{c}\tau)} \qquad (20)^2$$

where ϕ is a complex amplitude function of the disturbance. The disturbance velocity components are given by

$$\tilde{u} = \frac{\partial \tilde{\Psi}}{\partial y} = \bar{\phi}'(y)\, e^{i\bar{\alpha}(x-\bar{c}\tau)}, \qquad (21)^3$$

$$\tilde{v} = -\frac{\partial \tilde{\Psi}}{\partial x} = -i\bar{\alpha}\,\bar{\phi}(y)\, e^{i\bar{\alpha}(x-\bar{c}\tau)}. \qquad (22)$$

In a similar manner we may define a temperature perturbation as

$$\tilde{t}(x,y,\tau) = \bar{\xi}(y)\, e^{i\bar{\alpha}(x-\bar{c}\tau)}. \qquad (23)$$

Substituting the stream function perturbation and the temperature perturbation into equations (17), (18) and (19) we have

$$(U-\bar{c})(\bar{\phi}''-\bar{\alpha}^2\bar{\phi}) - U''\bar{\phi} = -\frac{i\nu}{\bar{\alpha}}\left[\bar{\phi}''''-2\bar{\alpha}^2\bar{\phi}''+\bar{\alpha}^4\bar{\phi}\right] - ig\beta\bar{\xi}', \qquad (24)$$

---

2 The convenient complex notation is used here. Physical meaning is attached only to the real part of the stream function, thus

$$Re(\Psi) = e^{\bar{c}_i\tau}\left[\bar{\phi}_r \cos\bar{\alpha}(x-\bar{c}_r\tau) - \bar{\phi}_i \sin\bar{\alpha}(x-\bar{c}_r\tau)\right]$$

3 Prime denotes differentiation with respect to the independent variable.

$$i\bar{\alpha}\left[(U-\bar{c})\,\bar{\xi}(y)-\bar{\phi}\,\frac{d(T-t_\infty)}{dy}\right]=\frac{k}{\rho C_p}\left[\bar{\xi}''(y)-\alpha^2\,\bar{\xi}(y)\right] \quad . \qquad (25)$$

It is appropriate to introduce dimensionless variables by dividing all of the quantities involved by characteristic quantities. The following dimensionless variables are introduced:

$$\eta = \frac{y}{\delta} \qquad \text{in which} \quad \delta = \sqrt{2}\,x/(Gr_x)^{\frac{1}{4}} ,$$

$$f' = U\,x/2\,\nu_\infty\sqrt{Gr_x} ,$$

$$\phi = \bar{\phi}\,x/2\,\nu_\infty\,\delta\sqrt{Gr_x} ,$$

$$\xi = \bar{\xi}/(t_w-t_\infty) ,$$

$$c = \bar{c}\,x/2\,\nu_\infty\sqrt{Gr_x} \quad .$$

Substituting these dimensionless quantities into equations (24), and (25) we obtain

$$(f'-c)(\phi''-\alpha^2\phi)-f'''\phi = -\frac{i}{\alpha G}\left[\phi''''-2\alpha^2\phi''+\alpha^4\phi\right]-\frac{i\beta\,\Delta t}{\alpha\,Fr}\,\xi' , \qquad (26)$$

$$(f'-c)\,\xi-\phi\,\mathcal{P}' = -\frac{i}{\alpha G\,Pr}\left[\xi''-\alpha^2\,\xi\right] , \qquad (27)$$

where G is a modified Grashof-number parameter appropriately describing the free-convection flow and defined as

$$2\sqrt{2}\,(Gr_x)^{\frac{1}{4}} \quad , \qquad Fr = 4\,\nu_\infty^2\, Gr_x / g\,\delta\, x^2$$

the Froude number and $Pr = \mu c_p / k$ the Prandtl number. Equation (26) is the equivalent of the Orr-Sommerfeld equation with an additional contribution due to the body-force term provided the Reynolds-number in the Orr-Sommerfeld equation is defined as $Re = U^* \delta / \nu_\infty$ where $U^* = 2\,\nu_\infty \sqrt{Gr_x} / x$. Equation (27) is the counterpart of the Orr-Sommerfeld equation for the energy amplitude function.

This fundamental system of equations for the velocity and temperature disturbances requires six boundary conditions for a solution. We require that all disturbances vanish at infinity. At the wall the normal and parallel disturbance velocities must vanish. Thus for an insulated wall the boundary conditions are:

$$\phi(0) = \phi'(0) = \zeta'(0) = 0 \quad ,$$

$$\phi \,,\ \phi' \,,\ \zeta \longrightarrow 0 \qquad \text{as} \quad \eta \longrightarrow \infty \quad , \qquad (28)$$

whereas for an isothermal wall the boundary conditions become

$$\phi(0) = \phi'(0) = \zeta(0) = 0 \quad ,$$

$$\phi \,,\ \phi' \,,\ \zeta \longrightarrow 0 \qquad \text{as} \quad \eta \longrightarrow \infty \quad . \qquad (29)$$

The problem of stability of the free-convection flow has now been reduced to an eigenvalue problem of equations (26) and (27) combined with either choice of boundary conditions equation (28) or equation (29). Eliminating ξ from equation (26) by appropriately differentiating equation (27), the two governing equations (26) and (27) can be reduced to the following single sixth-order differential equation in ϕ, as previously discussed by Plapp [19],

$$\left[\frac{i(f'-c)}{\alpha G P_r}+\frac{\alpha^2}{(\alpha G P_r)^2}\right]\left\{(f'-c)(\phi''-\alpha^2\phi)-f'''\phi+\frac{i}{\alpha G}\left[\phi''''-2\alpha^2\phi''+\alpha^4\phi\right]\right\}''$$

$$-\frac{if''}{\alpha G P_r}\left\{(f'-c)(\phi''-\alpha^2\phi)-f'''\phi+\frac{i}{\alpha G}\left[\phi''''-2\alpha^2\phi+\alpha^4\phi\right]\right\}'$$

$$+\left[(f'-c)-\frac{i\alpha^2}{\alpha G P_r}\right]^2\left\{(f'-c)(\phi''-\alpha^2\phi)-f'''\phi+\frac{i}{\alpha G}\left[\phi''''-2\alpha^2\phi''+\alpha^4\phi\right]\right\}$$

$$=\frac{i\beta\Delta t}{Fr\,\alpha}\left\{f''\vartheta'\phi+\left[(f'-c)-\frac{i\alpha^2}{\alpha G P_r}\right]\left[\vartheta''\phi-\vartheta'\phi'\right]\right\} \qquad (30)$$

Six constants, $A_1, \ldots, A_6$ are to be determined by the six boundary conditions as given by equation (28) or equation (29). For instance, the amplitude of the velocity fluctuation is

$$\phi = A_1\phi_1 + A_2\phi_2 + A_3\phi_3 + A_4\phi_4 + A_5\phi_5 + A_6\phi_6 \quad . \tag{31}$$

Thus the boundary conditions supply six homogeneous, linear, algebraic equations for the six constants $A_1, \ldots, A_6$. There is a non-trivial solution of this set of equations for $A_1, \ldots, A_6$ only if the determinant of the coefficients of A_n is zero. Since the coefficients of ϕ, ξ, and its derivatives are functions of α, c, αG, and Pr for a given velocity profile, setting the determinant $D(\alpha, c, \alpha G, Pr) = 0$ gives a functional relation for these quantities. The $\alpha, c, \alpha G, Pr$, which satisfy this relation, are the eigenvalues.

To solve completely the eigenvalue problem of the above determinant is a difficult task without a high-speed electronic computing facility.

Thus the problem is limited here to determining the nature of the stability of laminar free convection in a viscous fluid when the coupling term in equation (26) due to the temperature fluctuation is neglected. S. Ostrach [25] showed that the body force does not directly affect the stability for natural convection. However, for the complete coupled problem in the free-convection case, justification of

this assumption still remains open.

By virtue of dropping the coupling term we need only equation (26) in the form:

$$(f'-c)(\phi''-\alpha^2\phi)-f'''\phi=-\frac{i}{\alpha G}(\phi''''-2\alpha^2\phi''+\alpha^4\phi)\,. \tag{32}$$

The amplitude function ϕ can thus be represented by linearly independent solutions ϕ_1, ϕ_2, ϕ_3, and ϕ_4 and may be written as

$$\phi(\eta)=A_1\phi_1+A_2\phi_2+A_3\phi_3+A_4\phi_4\,. \tag{33}$$

The boundary conditions for the reduced equation are

$$\begin{aligned}&\phi(0)=\phi'(0)=0\,,\\ &\phi,\ \phi'\longrightarrow 0 \quad \text{as} \quad \eta\longrightarrow\infty\,.\end{aligned} \tag{34}$$

The property of the solutions of equation (32) for large values of αG (or equivalently αRe) has been investigated in detail by previous researchers (cf. Lin [26], ch. 8). The solutions ϕ_1 and ϕ_2 are classified as inviscid solutions, and ϕ_3 and ϕ_4 as viscous solutions. For the limiting value of $\alpha G\longrightarrow\infty$ the inviscid solutions have existent values throughout the flow field whereas the viscous solutions vanish almost everywhere except in the vicinity of the critical points where the essential influence of viscosity on the disturbances comes into effect.

1.) The Inviscid Solutions

The inviscid solutions are expected to be valid for large values of the modified Grashof-number parameter. In this limit the coefficient $1/\alpha G$ of the right-hand side of equation (32) becomes so small that the viscous terms on the right-hand side of the equation can be neglected, giving the inviscid disturbance equation:

$$(f'-c)(\phi''-\alpha^2\phi)-f'''\phi=0 \quad . \tag{35}$$

The boundary conditions are

$$\begin{aligned} &\phi = 0 \qquad \text{at} \quad \eta = 0 \quad , \\ &\phi = 0 \qquad \text{as} \quad \eta \longrightarrow \infty \quad . \end{aligned} \tag{36}$$

For neutral oscillations $(c = c_r - ic_i \; , \; c_i = 0)$ $f'-c$ must vanish at some position. The critical points, where $f'=c$, are singularities of equation (35) which arise as a result of neglecting terms in $1/\alpha G$. The velocity distribution in the free-convection flow as shown in Fig. 1 has two critical points at which $f'-c$ vanishes. The inner critical point η_{ci} is located nearest the wall for which f'' is positive whereas the outer critical point η_{co} is located outside the maximum velocity near the ambient fluid for which f'' is negative. By the use of the method of Frobenius we can obtain two independent solutions near each critical point. The solutions in the neighborhood of η_{ci} are given in the form:

$$\phi_{1i} = (\eta - \eta_{ci}) \sum_{n=0}^{\infty} a_n (\eta - \eta_{ci})^n \quad , \tag{37}$$

$$\phi_{2i} = \sum_{n=0}^{\infty} b_n (\eta - \eta_{ci})^n + K_i \phi_{1i} \log(\eta - \eta_{ci}) \quad , \tag{38}$$

for $\eta > \eta_{ci}$. The way of choosing the proper branch of $\log(\eta - \eta_{ci})$ for $\eta > \eta_{ci}$ has been established by Tollmein [27] and other workers (see Lin [26] , p. 130). If $f''_{ci} > 0$ then $\log(\eta - \eta_{ci}) = \log|\eta - \eta_{ci}| - i\pi$ where f''_{ci} refers to the first derivative of the velocity profile at the inner critical point. In a similar manner we obtain a second pair of solutions about the outer critical point:

$$\phi_{1o} = (\eta - \eta_{co}) \sum_{n=0}^{\infty} c_n (\eta - \eta_{co})^n \quad , \tag{39}$$

$$\phi_{2o} = \sum_{n=0}^{\infty} d_n (\eta - \eta_{co})^n + K_o \phi_{1o} \log(\eta - \eta_{co}) \quad , \tag{40}$$

for $\eta > \eta_{co}$. Analysis of the proper branch for the $\log(\eta - \eta_{co})$ when $\eta < \eta_{co}$ and $f''_{co} < 0$ results in $\log(\eta - \eta_{co})$ $= \log|\eta - \eta_{co}| + i\pi$

In the neighborhood of the critical layer ($f' - C$) may be expanded in the following Taylor series:

$$(f' - C) = f''_c (\eta - \eta_c) + \frac{1}{2!} f'''_c (\eta - \eta_c)^2 + \cdots \quad . \tag{41}$$

Substituting equation (41), with ϕ_{1i} and ϕ_{2i}, into equation (35) we obtain the following constants for the solutions of the inner critical layer:

$$K_i = f_{ci}'''/f_{ci}''$$

$$a_0 = 1\ ,\quad a_1 = f_{ci}'''/2f_{ci}''\ ,\quad a_2 = \alpha^2/6 + f_{ci}''''/6f_{ci}''\ ,\ \ldots\ ;$$

$$b_0 = 1\ ,\quad b_1 = 0^4\ ,\quad b_2 = \alpha^2/2 + f_{ci}''''/2f_{ci}'' - (f_{ci}'''/f_{ci}'')^2\ ,\ \ldots\ .$$

Similarly, substituting equation (41), with ϕ_{1o} and ϕ_{2o}, into equation (35) we obtain the following constants for the solutions of the outer critical layer:

$$K_o = f_{co}'''/f_{co}''$$

$$c_0 = 1\ ,\quad c_1 = f_{co}'''/2f_{co}''\ ,\quad c_2 = \alpha^2/6 + f_{co}''''/6f_{co}''\ ,\ \ldots\ ;$$

$$d_0 = 1\ ,\quad d_1 = 0\ ,\quad d_2 = \alpha^2/2 + f_{co}''''/2f_{co}'' - (f_{co}'''/f_{co})^2\ ,\ \ldots\ .$$

For sufficiently large distances from the wall (large η) the derivations of the velocity profile vanish and equation (35) reduces to

$$\phi'' - \alpha^2\phi = 0\ . \qquad (42)$$

---

4 We concluded $b_1 = 0$ since the coefficients of b_1 lead to ϕ_1 which is already a solution.

The general solutions are $\phi = e^{\pm \alpha \eta}$. Since we have a boundary condition $\phi = 0$ as $\eta \longrightarrow \infty$, the only admissible solution is

$$\phi = e^{-\alpha \eta} .$$

ii.) Viscous Solutions

A second pair of solutions ϕ_3 and ϕ_4 , i.e., the viscous solutions, must be obtained from equation (32). The solutions ϕ_3 and ϕ_4 are represented asymptotically for large values of G by solutions of the simplified stability equation. In order to deduce the simplified stability equation, it is convenient to introduce a new variable Z defined by

$$Z = \frac{\eta - \eta_c}{\epsilon} \qquad (43)$$

The parameter ϵ produces a stretching of the coordinate system and is generally considered small for neutral oscillations. The choice of ϵ is arrived at by an order of magnitude consideration of the terms ϕ'''' and $i \alpha G (f' - C) \phi''$ in equation (32) in the neighborhood of η_{ci} and η_{co} , respectively. This consideration yields $\epsilon_i = (\alpha G f''_{ci})^{-\frac{1}{3}}$ in the neighborhood of η_{ci} and $\epsilon_o = (-\alpha G |f''_{co}|)^{-\frac{1}{3}}$ in the neighborhood of η_{co} , when $(f' - c)$ is replaced by the first term of its Taylor series expansion.

Substituting the new variable for the inner-critical-layer solution $Z_i = (\alpha G f''_{ci})^{\frac{1}{3}} (\eta - \eta_{ci})$ into equation (32) we obtain as a first approximation

$$i\frac{d^4\phi}{dz_i} + z_i\frac{d^2\phi}{dz_i^2} = 0 \quad . \tag{44}$$

The solutions of this equation are universal, independent of the basic flow. The solutions are

$$\phi_1 = 1 \,,$$

$$\phi_2 = z_i \,,$$

$$\phi_3 = \int_{\infty}^{z_i}\int_{\infty}^{z_i} z_i^{\frac{1}{2}}\, H_{\frac{1}{3}}^{(1)}\left[\frac{2}{3}(iz_i)^{\frac{3}{2}}\right] dz_i\, dz_i \,, \tag{45}$$

$$\phi_4 = \int_{-\infty}^{z_i}\int_{-\infty}^{z_i} z_i^{\frac{1}{2}}\, H_{\frac{1}{3}}^{(2)}\left[\frac{2}{3}(iz_i)^{\frac{3}{2}}\right] dz_i\, dz_i \,,$$

where $H_{\frac{1}{3}}^{(1)}$ and $H_{\frac{1}{3}}^{(2)}$ denote Hankel functions of the first and second kind of order one-third respectively.

Similarly, when the independent variable for the outer critical layer $z_o = (-\alpha G|f_{co}''|)^{\frac{1}{3}}(\eta - \eta_{co})$ is substituted into equation (32), we obtain

$$i\frac{d^4\phi}{dz_o^4} + z_o\frac{d^2\phi}{dz_o^4} = 0 \quad . \tag{46}$$

This equation is formally identical with equation (44) for the inner critical layer solution. The solutions of equation (46) are hence the same as given by equation (45) with z_i replaced by z_o ; only the integration limit must be properly chosen.

iii.) Formulation of the Eigenvalue Problem

The disturbance amplitude function for the uncoupled problem is the sum of the four linearly independent solutions;

$$\phi = B_1 \phi_1 + B_2 \phi_2 + B_3 \phi_3 + B_4 \phi_4 \quad . \tag{47}$$

The solutions ϕ_1 , ϕ_2 , ϕ_3 , and ϕ_4 are subject to the boundary conditions already stated in equation (36). Since the Hankel function $H_{\frac{1}{3}}^{(2)}$ goes to infinity as $z \longrightarrow \infty$ it does not satisfy the boundary condition at infinity. Therefore, ϕ_4 should not contribute to the solution, and we have

$$\phi = B_1 \phi_1 + B_2 \phi_2 + B_3 \phi_3 \quad . \tag{48}$$

Applying the boundary conditions we obtain a set of algebraic equations for the constants B_1 , B_2 , and B_3 ;

$$\begin{aligned} B_1\phi_1(0) + B_2\phi_2(0) + B_3\phi_3(0) &= 0 \quad , \\ B_1\phi_1'(0) + B_2\phi_2'(0) + B_3\phi_3'(0) &= 0 \quad , \\ B_1\phi_1(\infty) + B_2\phi_2(\infty) + B_3\phi_3(\infty) &= 0 \quad . \end{aligned} \tag{49}$$

However, the Hankel function $H_{\frac{1}{3}}^{(1)}$ vanishes as $z \longrightarrow \infty$, therefore, equation (49) becomes

$$\begin{aligned} B_1\phi_1(0) + B_2\phi_2(0) + B_3\phi_3(0) &= 0 \quad , \\ B_1\phi_1'(0) + B_2\phi_2'(0) + B_3\phi_3'(0) &= 0 \quad , \\ B_1\phi_1(\infty) + B_2\phi_2(\infty) &= 0 \quad . \end{aligned} \tag{50}$$

Choosing ϕ_1 so that $\phi_1(\infty) = 0$, we have $B_2 = 0$ and the system of equations reduces to

$$B_1\phi_1(0) + B_3\phi_3(0) = 0 \quad ,$$
$$B_1\phi_1'(0) + B_3\phi_3'(0) = 0 \quad . \tag{51}$$

For a non-trivial solution of B_1 and B_3 the following must be true:

$$\begin{vmatrix} \phi_1(0) & \phi_3(0) \\ \phi_1'(0) & \phi_3'(0) \end{vmatrix} = 0 \quad . \tag{52}$$

This provides the boundary-condition equations

$$\frac{\phi_1(0)}{\phi_1'(0)} = \frac{\phi_3(0)}{\phi_3'(0)} \quad . \tag{53}$$

Substituting $z_{i0} = -\eta_{ci}/\epsilon_i$ for the inner-critical point into equation (53) we obtain

$$-\frac{\phi_1(0)}{\eta_{ci}\phi_1'(0)} = \frac{\phi_3(z_{i0})}{z_{i0}\phi_3'(z_{i0})} \quad . \tag{54}$$

This equation is the conventional equation used in the analysis of the stability of boundary-layer profiles. The right-hand side of equation (54) is the viscous solution and only a function of z_{i0}, whereas the left-hand side is the inviscid solution and a function of α and C only. Therefore a solution of this equation gives

discrete combinations of α , C , and Z_{i_0} .

Equation (54) can be written in the following form:

$$E(\alpha, c) = F(z_{i_0}) \quad . \tag{55}$$

In this equation $F(z_{i_0})$ is the so-called Tietjens function [28] expressed as

$$F(z_i) = \frac{\int_{\infty}^{z_{i_0}} \int_{\infty}^{z_i} z^{\frac{1}{2}} H^{(1)}_{\frac{1}{3}} \left[\frac{2}{3}(iz)^{\frac{3}{2}}\right] dz \; dz_i}{z_{i_0} \int_{\infty}^{z_{i_0}} z^{\frac{1}{2}} H^{(1)}_{\frac{1}{3}} \left[\frac{2}{3}(iz)^{\frac{3}{2}}\right] dz} \quad . \tag{56}$$

A solution of equation (55) is most conveniently obtained by a graphical method, i.e., the intersections of the calculated curves from the inviscid solution $E(\alpha, C)$ and the Tietjens function give the desired eigenvalues. From the definition of z_{i_0} the modified Grashof parameter, G , can be found and hence an indifference curve will be established. The numerical procedure used in obtaining the indifference curve is described in Appendix A.

a.) <u>A Solution Considering the Outer Critical Point</u>

Let us now consider a procedure for the outer-critical point similar to that presented above. Before proceeding, it must be emphasized that an analysis of this type gives only a rough approximation of the desired solution since only terms of order ϵ_0 are retained. Nevertheless, this speculative procedure was carried out for

the following reasons:

1. The numerical results obtained for equation (55) based on the inner-critical point produced unreasonably high critical values for the modified Grashof-number parameter.

2. Plapp [19], in his calculations of an indifference curve for air ($P_r = 0.72$) using a polynomial representation[5] of the free-convection velocity profile, also found unreasonably high values for the critical Rayleigh number. Plapp also performed similar calculations on the exact profile as given by Ostrach [23]. The latter calculations, however, are to be seriously doubted since substantial numerical errors were introduced.

3. The free-convection velocity profile is similar to a two-dimensional unsymmetrical jet streaming near a parallel wall. It is known that calculations for two-dimensional jet profiles at large distance from the core of the jet, where the velocity profile almost vanishes, lead to very low critical Reynolds number.

4. Experimental evidence shows that the free-convection layer becomes unstable near the outer critical layer first. This instability appears to play a significant role in the transition of the free-convection layer from laminar to turbulent flow. This point will be discussed in more detail in a later section.

[5] $$\bar{u} = \begin{cases} \frac{243}{64}\eta\left(1-\frac{9}{16}\eta\right)^2 , & 0 \le \eta \le \frac{16}{9} \\ 0 , & \eta \ge \frac{16}{9} \end{cases}$$ (See Squires [29])

5. The free-convection velocity profile contains an inflection point outside the maximum velocity near the ambient fluid. Generally, inflection points in the velocity profile are very significant because, when present, a velocity profile is more unstable than that without an inflection point. Such an inflectional instability has been discussed by Gregory, Stuart and Walker [30] on the experiments performed on a swept-back wing having a similar velocity profile as that obtained in the flow on a rotating disk. Also Boltz, Kenyon, and Allen [31] encountered a similar velocity profile in the experiments performed to determine the effect of swept-back angle on the boundary-layer stability of an untapered wing.

The boundary condition equation is given by equation (53). Substituting the variable $z_{oo} = -\eta_{co}/\epsilon_o$ for the outer critical point into the left-hand side of equation (53) we obtain

$$-\frac{\phi_1(0)}{\eta_{co}\,\phi_1'(0)} = \frac{\phi_3(z_{oo})}{z_{oo}\,\phi_3'(z_{oo})} \qquad (57)$$

This equation is similar to equation (54) and can be written in the form

$$\mathcal{E}(\alpha, c) = \mathcal{F}(z_{oo}) \qquad (58)$$

the only significant change being that z_{io} is replaced by z_{oo} . The variables z_{io} and z_{oo} differ by a minus sign. Thus the

Tietjens function becomes

$$F(z_\infty) = \frac{\int_{\infty}^{z_{\infty}} \int_{\infty}^{z_0} z^{\frac{1}{2}} H_{\frac{1}{3}}^{(1)} \left[\frac{2}{3}(iz)^{\frac{3}{2}}\right] dz\, dz_0}{z_{\infty} \int_{\infty}^{z_{\infty}} z^{\frac{1}{2}} H_{\frac{1}{3}}^{(1)} \left[\frac{2}{3}(iz)^{\frac{3}{2}}\right] dz} \qquad (59)$$

Noting this significant difference equation (58) can now be solved by using exactly the same procedure as indicated previously for the inner-critical point.

Experimental Equipment

The experiments were performed in a water tank 3 feet wide, 5 feet deep and 7 feet long. The vertical heated plate was made of brass 31 inches wide, 60 inches long and 0.25 inches thick. The brass plate was one side of a double-wall construction which was mounted in a bakelite frame as shown in Fig. 2. The entire brass plate was heated by two circuits of No. 22 Nichrome wire. A Variac controlled the current of the 0-15 ampere circuits within 0.1 ampere. The wire passed through Stoupakoff insulating tubing as it was wound into a parallel grid covering the width of the plate as shown in Fig. 3. The spacing of the grid was one inch. The heating wires were firmly pressed against the brass plate by Spun-Fiberglass packing which also kept the heat loss a minimum. The packing was contained and made watertight within the bakelite frame by a second wall made of aluminum. The

aluminum wall was the same size as the brass wall but was not heated. The double-wall structure was submerged vertically midway the length of the tank and permanently fastened to the tank.

In order to facilitate the analysis of experimental results, a grid consisting of 5 cm by 5 cm squares was marked on the brass plate starting at 30 cm from the leading edge. The temperature of the plate was determined from thirteen thermocouples imbedded in the plate at the locations shown in Fig. 4. Details of an imbedded thermocouple are shown in Fig. 5.

All thermocouples used in this experiment had a copper-constantan junction. The temperature field in the free-convection layer created by the heated wall was measured by a thermocouple probe as shown in Fig. 6. The thermocouple probe was attached to a traversing mechanism, as shown in Fig. 7, that had an accuracy of traverse of 0.0005 inches.

The thermocouple reading were recorded by a Leeds and Northrup-Speedomax recorder. The actual temperatures were printed on temperature-coordinate paper having a scale of 0°C to 50°C, and running at the speed of 64 inches per hour. The recorder printed a temperature point once every four seconds. By this read-out device we could quickly identify when the wall temperature had reached the desired isothermal condition and whether it was being maintained throughout an experimental run.

For the study of the stability and transition of the free-

convection layer the flow visualization technique of dye injection was used. Dye was injected smoothly through three different types of dye rakes. For plan-view observation of the flow development, hypodermic dye rakes as shown in Fig. 8 allowed black dye or black and red dye to be injected into the free-convection layer. A comb-type dye rake or an individual hypodermic needle was used for side-view observations. The comb-type dye rake emitted several colors of dye at various distances from the wall in a single plane so as to identify different flow paths at various distances from the wall. The flow experienced no ill effects from the dye rakes inserted into the flow field 6 inches from the leading edge.

For most of the observations Nigrosine black dye was used; a red solution of acid chrome blue dye in water was used as the second dye for several flow pattern observations. In addition, brilliant yellow, brilliant green, and orange G dyes were also used to give contrast between dye streaks. The difference in density between colored and clear water was negligible.

Flow phenomena were analyzed from both motion pictures and still photographs. The motion pictures were taken with a Bolex 16-mm movie camera at speeds of 16 frames per second or 32 frames per second. The movie camera was calibrated by photographing a time display on the Berkeley Universal Eput and Timer. The still photographs were taken with an Exakta 35-mm camera.

Experimental Procedure

In order to perform a carefully controlled experiment it was necessary for the brass plate to reach a uniform, steady-state temperature. Generally, the Variac control unit was adjusted to a given power input three to five hours prior to a run in order to attain this condition. Steady-state wall temperature was evidenced after a time period on the temperature recorder. The temperature recorder was standardized several times during this period to be able to account for any changes in ambient conditions.

Temperature profiles were obtained by means of a thermocouple probe. The thermocouple probe was attached to the traversing mechanism and submerged into the tank. The probe was adjusted to a desired distance from the leading edge. The normal-distance "zero" reading was obtained by adjusting the micrometer until the thermocouple touched the plate. The "zero" reading was recorded and used as a reference reading for successive micrometer movements. The thermocouple probe was retracted away from the wall at the intervals of 0.0050 inches until the temperature recorder registered a constant ambient reading, t_∞. Thereupon, the path was traced back at the same intervals to the "zero" reading, at the wall. The thermocouple junction had a thickness of 0.0060 inches. Therefore, the normal distances recorded from the micrometer were corrected by 0.0030 inches. This assumed the contact point of copper and constantan to be midway the thickness of the junction.

The wall-temperature readings were recorded directly from the imbedded thermocouples. For each reading obtained from the thermocouple probe an entire set of wall temperature readings was recorded. These wall-temperature readings were then averaged and used as t_w .

When flow-pattern investigations were made, the thermocouple probe was positioned at a sufficiently large normal distance from the wall. Thus, only the ambient temperature and the wall temperature were recorded. For flow-pattern investigations dye was permitted to the flow through the dye rakes after the plate had reached a uniform, steady-state temperature. Careful control was required of the dye flow so as not to shoot it into the flow and disturb the flow field. The flow field passing the hypodermic needles actually drew the dye into the free-convection layer. As the dye patterns developed, still as well as motion pictures were taken; the still pictures for the purpose of reproduction, the motion pictures for the purpose of analysis of the flow developments.

The dye patterns which were recorded on film were then projected on a screen whereupon they were subject to analysis, i.e., wave lengths, leading edge distances, and wave propagation speeds were measured.

This procedure was followed for numerous runs at various temperature differences between the wall and ambient temperature. The temperature differences were always small as required for comparison with theory. The experimental runs were performed at temperature differences up to about ten degrees.

Results, Observations and Discussion

A typical result of the temperature-profile measurements is shown in Fig. 9. In this figure a sharp temperature decrease is noticed very near the wall. This decrease takes place in the region up to approximately $y = 0.008$ inches. This anomaly might be attributed to the conduction process taking place across the thin layer of fluid between the thermocouple and the wall. Very close to the wall the fluid moves very slowly such that a conduction process takes place rather than a convective process, hence the temperature recorded is that of an almost still liquid. Since conduction in a liquid is very poor, the recorded temperature is slightly lower than the streaming fluid within a short distance away. For the distance $y > 0.008$ inches this effect apparently becomes negligible.

As mentioned in the Procedure, the wall temperature was obtained by averaging the temperatures recorded from the imbedded thermocouples. This average wall temperature was used because, first, it agreed well in nearly all instances with the temperature obtained by extrapolating the temperature profile data to the wall (see Fig. 9). Secondly, the local wall temperature also agreed well with the overall average wall temperature. A typical wall temperature distribution is given in Fig. 10. Near the leading edge of the wall there is a flow-wise temperature gradient in the wall. Cause of the lower wall temperature near the leading edge of the wall is the circulatory motion of the fluid in the tank, i.e., cold fluid is constantly drawn into the free-convection layer near the leading edge. Thus, a more intensive cooling

effect was caused, resulting in the lower wall temperature near the leading edge. The wall temperature, nevertheless, approaches an almost uniform value rapidly and the effect due to a small gradient near the leading edge is neglected. The two temperature readings obtained in the first five inches are not included in the average wall temperature.

Knowing the wall temperature and the ambient temperature Fig. 9 can be converted into a dimensionless plotting, ϑ vs. η . The fluid properties included in the definition of the dimensionless variable η are based on the ambient temperature, t_∞ . Since the temperature difference between the wall and the ambient temperature was small, the values of η did not change appreciably when the fluid properties based upon the wall temperature were used, instead. Therefore, this is an arbitrary and inessential choice as long as the temperature difference remains small.

Experimental temperature profiles for the ϑ vs. η plotting are shown in Fig. 11. The experimental temperature profiles are compared with the theoretical temperature profiles calculated by Ostrach [23] . Agreement between the theoretical and experimental temperature profiles is quite good.

Equation (55) was solved for the velocity profile as shown in Fig. 1 for the Prandtl number 10. A velocity profile calculated for the Prandtl number 10 was used since it was assumed that it would provide an upper bound for a good representative velocity profile for the free-convection flow in water. The solution of equation (55) is plotted in

Fig. 12. Combinations of c, α, and $-z_{i_0}$, obtained from intersection points in Fig. 12 are given in Table 1. The modified Grashof-number parameter, G, calculated from z_{i_0} is also given in Table 1. The indifference curve gives a minimum value for G of 3.46×10^5 corresponding to $c = 0.0235$ and $\alpha = 0.875$. Fig. 14 shows a similar plotting, in which G and c are presented as abscissa and ordinate, respectively. Fig. 15 shows the inviscid function ϕ_i, for a neutral oscillation.

The solution of equation (58) is presented graphically in Fig. 16. Points of intersection are given in Table 2 and presented in Fig. 17, along with the indifference curve obtained for the inner-critical point. A marked shift in a portion of the neutral stability curve is noted. In spite of a quite suspectible approximation procedure in regard to the velocity profile in the stability calculation, somewhat more reasonable values for the modified Grashof-number parameter were obtained and a more reasonable critical value is implied in these results. The lowest value of G obtained was $G = 5040$ at $c = 0.005$ and $\alpha = 1.5$.

For various temperature differences ranging from 3 to 8 degrees, the measured wavelengths, wave velocities and distances from the leading edge were transformed into the nondimensional quantities c, α, and G, respectively. These experimental results are plotted in Fig. 17 and Fig. 18. The experimental values of G were in a region bracketed by $G = 500$ and $G = 700$. Although the agreement between the measured minimum modified Grashof-number parameter and that predicted by theory based on the inner critical layer is poor, there is

a fairly good agreement for the α , c combinations corresponding to the predicted minimum value of G. That is the values obtained from the inner-critical layer theory were $c = 0.0235$ and $\alpha = 0.875$ and the over-all average of the measured quantities were $\alpha = 0.673$ and $c = 0.0321$.

Comparing the experimental results with the c, α , and G combinations obtained from equation (58), a better agreement in the G parameter is obtained 8 to 10 times less than that predicted by the theory. But the α , C combinations corresponding to this G value provide less satisfactory agreement

Within the distance approximately 40 cm from the leading edge, thin black dye streaks move up the surface of the wall very slowly without showing any indication of breaking. In this distance from the leading edge, the flow was laminar and remained approximately so regardless of the temperature difference imposed between the wall and the ambient fluid up to about 10 degrees. This laminar flow pattern can be seen in the lower portion of Fig. 19 or Fig. 20 in which the flow direction is from bottom to top. The laminar flow portion could be extended almost to the entire length of the wall for the temperature difference approximately 2 degrees or less. Temperature differences of this much magnitude, however, were not used since the flow would become turbulent as a result of the disturbances caused at the free surface at the top rather than by a natural transition process itself.

The dye streaks as shown in Fig. 19 for $\Delta t = 6.44$ show a laminar flow pattern up to approximately 55 cm from the leading edge. At 55 cm from the leading edge a faint two dimensional dye accumulation begins to appear. A rather concentrated, more definable dye line is seen at 60 cm, thus giving a wave length approximately 5 cm. The wave length was obtained by averaging several measurements across the plate since there was a certain amount of irregular transverse waviness exhibited by the wave front. This transverse waviness, however, was not unexpected since the disturbance waves occurred naturally and were not produced by an artificial means of any geometrical regularity or at a specific frequency. Since the disturbance waves were formed arbitrarily in time as well as in space, a certain portion of a wave moving downstream could be engulfed by a second wave which started at a slightly higher x-location.

As we proceed upwards with the flow in Fig. 19, it is noted that a "splitting" of the dye streaks begins to take place at the wave front located at x = 60 cm. The splitting of the dye streaks appears because there is a secondary twisting of the dye streak near the plate surface. Although this twisting of the dye streak occurs, the free-convection layer still appears to be in a somewhat later stage of a still laminar flow, or in the initial stages of transition.

Before proceeding further in the discussion of the overall picture of transition which takes place in the free-convection layer, a good deal of insight can be obtained by examining a single dye

streak in plan and side views. Fig. 25 shows the developmental process of a single dye streak taking place at various normal distances from the wall at $\Delta t = 7\ ^{\circ}C$. The $y = o$ dye streak shown in Fig. 25 (a) illustrates the laminar flow portion at the extreme left which looks quite two dimensional. As the flow proceeds the "splitting" process begins to take place. After the appearance of the initial splitting the dye streak is still in a laminar state, although it is swept down stream by the mean velocity in a twisting manner. Portions of the dye streak, as it is being twisted, are twisted up away from the wall and into a region of slightly higher velocity, whereas some of the dye sticks to the wall. At the same time the dye streak is also being carried downstream by the mean flow and continues to concentrate at a second discrete place along its path. The places of the concentration and the so-called splitting are seen in Fig. 25 (g) which shows a side view of what actually occurs to a dye streak riding on the surface of the wall. The dye streak rolls up to form a vortex. This type of vortex rolling-up was verified by Hama [6] for the boundary-layer flow over a flat plate. In all instances observed, the vortex continues to roll up and appears in the plan view as a highly concentrated dye spot for a single dye streak or as a concentrated dye line for several streaks. Such a concentrated dye line is observed in Fig. 19 at $x = 60$ cm. This concentrated dye line continues to be concentrated and the wave amplified until a second splitting process occurs. The vortex, which appeared

to be mainly two-dimensional, now begins to take on some three-dimensional character. Yet, from a side view it appears as a nearly two-dimensional rolling-up, but plan view clearly shows the distortion into a three-dimensional formation. Before this three-dimensionality proceeds very far downstream, several dye streaks all having the same character join in forming a vortex loop. The edges of the dye streaks, which form the legs of the loop, are very cloudy and immediately burst into a highly random motion indicating the burst of a turbulence spot. Any further observation is completely obscured by the dye clouds due to the random motion.

Basically this same type of flow phenomenom is observed for various temperature differences. This is clearly shown in Figs. 20, 21, 22, 23, and 24, which are representative pictures of all the flow observations photographed. No marked difference could be detected for the flows at higher temperature differences except that the wave fronts would appear to be quite straight and not have a great amount of transverse waviness. Transverse waviness at high temperature differences did not have sufficient time to develop because the onset of turbulence moved down the plate and occurred very quickly.

Let us now return to the sequential photos of a single dye streak in Fig. 25. As the hypodermic needle was retracted from the wall the dye streak slowly left the surface. It should be noted here that the normal readings are actual micrometer adjustments and correspond only approximately to the true normal distance from the

wall at which the dye streak is located. The precise location of the dye streak, however, need not concern us here, as long as we know that it is increasing in distance from the wall. In Fig. 25 for y = 0.030 and 0.060 inches, respectively, the dye streaks indicate the same type of twisting, and vortex concentrating flow as previously discussed for the dye streak at $y = o$. At $y = 0.090$ inches and greater, corresponding to $\eta = 0.61$ and greater, the observed dye pattern shows a considerably different flow phenomenom occuring and only vaguely resembles the flow pattern previously observed in Fig. 25 (a),(b) and (c). The regularity of the dye-concentration points seems to be lost completely. The motion now takes on a highly intensified irregular lengthwise wave motion. This observation is informative as it indicates that a different type of mechanism may be taking place. At $\eta = 0.61$ the velocity is almost at its maximum. Hence, the dye streak is now in a region where the viscosity does not play a major role but the inflectional instability makes its presence known.

In order to clarify the flow phenomenom observed by a single dye streak in plan view, the dye streak was observed in side view at various normal distances from the wall, (see Fig. 26). What was observed in Fig. 26 (a) (b) (c) (d) and (e) seemed to be that as expected the dye streak rolled up into a vortex and continued to roll while being carried downstream by the mean flow until the final break-down occurred. But as we proceeded to retract the dye streak farther

away from the wall, a counter-clockwise rotating vortex (rolling out into the ambient fluid) appeared at the crest of the main vortex formed near the plate. After several runs of single dye streak observation at various distances from the wall, it was noticed that the counter-clockwise rolling of the dye at the crest of the vortex appeared with consistent regularity. In order to observe this condition further, the dye comb was used to give dye streaks at various normal distances from the wall at the same time. The use of this type of dye-injection device produced rather unexpected results as shown in Fig. 26 (g). Fig. 27 shows the vortex formation of two dye streaks. A red-dye streak rides up along the surface of the wall, whereas a blue-dye streak flows upwards outside the maximum velocity in the layer. It is immediately evident that a double-row vortex system arises. The red-dye streak rolls up on the wall similar to that observed in a conventional boundary-layer flow over a flat plate, whereas the blue dye outside the maximum velocity rolls outward having a counter-clockwise rotation in the opposite direction to that of the vortex formed on the plate. This vorticity distribution in the free-convection layer confirmed the speculation brought forth by Fujii [18], although the actual phase relation between the two vortex rows differs from his sketch. Perhaps, more interesting to note is that Fales [7] observed a similar phenomencn when a jet of clear water issued into a bath of dyed water. A strong similarity exists between a jet velocity profile and the velocity profile obtained for a free-convection layer.

The free-convection velocity profile is likened to a two-dimensional unsymmetrical jet streaming near a parallel wall with still fluid outside its outer edge.

The rolling up of the outer vortex begins to occur very near the leading edge. A disturbance wave front can be seen very near the leading edge in Fig. 28. It shows a plan view of a red-wave front between 45 and 50 cm from the leading edge. (Note the change in dye colors for plan view: Black dye flows up along the surface of the plate and red dye outside the maximum velocity). When the red wave front appears, the black dye streaks in the rear riding up the surface of the plate remain laminar. Several wave fronts of the red dye are observed in contrast to generally only two or at most three wave fronts observed of the dye streaks on the surface of the plate as previously discussed. As the wave progresses upwards along the plate and is amplified, the red dye line becomes more concentrated. The concentrated red dye line exhibits the same type of vortex rolling up as before until again the vortex loop is developed and eventual breakdown occurs. This breakdown observed in the outer layer occurs at a distance from the leading edge when the inner layer is still laminar or only shows signs of initially entering transition. The outside rolling vortex is very strong and impresses its effect onto the inner layer. The inner layer is actually disturbed by the large amplification of the outside disturbance wave and by its development to final breakdown. Hence, the inside wave is provoked by the highly

unstable motion occurring outside the maximum velocity. This occurrence must result from the strong instability due to the inflection point in the velocity profile located outside the maximum velocity. Its effect is to overtake the flow completely and control its behavior. This type of instability was clearly manifested in the breakdown of the free-convection layer from laminar to turbulent flow.

The outside wave so dominated the flow that it impressed its wave length onto the wave disturbance in the inner layer. The outside wave is completely established even before the inside wave begins to show signs of a vortex rolling up. This is clearly seen in Figs. 27 and 28. Results of the measurements obtained from the outside wave disturbance are plotted in Fig. 29. These experimental points fall in the same region on the α, G plot as did the previously measured data obtained from the wave very near the wall.

CONCLUSION

Theoretical as well as experimental investigations of the instability and transition in the free-convection layer along a vertical flat plate have led to the following conclusions:

1. In the process of natural transition in the free-convection layer a double-row vortex system arises. One of the two rows of vortices takes place near the surface and inside the maximum velocity rolling toward the surface, whereas the second row of vortices forms outside the maximum velocity rolling out into the ambient fluid. The double-row vortex system is the consequence of the particular velocity profile in the free-convection layer for which two critical layers exist one on each side of the velocity maximum.

2. It has been experimentally established that the instability due to the outer critical layer is predominant and sets in first, well in advance of the onset of any possible instability due to the inner critical layer. In fact, the instability in the outer layer is so strong and amplified rapidly to form discrete vortices. The outside vortices completely control the behavior of the flow developments and impress their effect onto the more stable inner layer near the surface, causing its instability. The initial instability takes place at the modified Grashof number approximately 600.

3. The above observation explains why the critical Grashof-number parameter experimentally obtained here and in the other literature is so much below the theoretical Grashof-number parameter 3.46×10^5 which is computed based upon the instability of the inner critical layer. Such an instability simply does not come into the picture.

4. The theoretical calculations for the minimum Grashof number based on the inner-critical layer for a velocity profile corresponding to a Prandtl number of 10 produces values of Grashof number of the same order of magnitude as obtained by Plapp [19] for a velocity profile corresponding to a Prandtl number of 0.72.

5. The instability calculation based upon the consideration of the outer critical layer shows a drastic reduction of the theoretical Grashof number to the order of 10^3. Experimental evidence tends to agree better with this reduction obtained in the present paper from the linearized approximation for the outer critical layer. It is felt that, because of the approximate procedure, agreement with the experiment is still poor, although it is far better than when compared with the stability curve based upon the inner critical layer. Improvement of the theoretical treatment is desired in dealing with the instability due to the outer critical layer.

6. Small perturbation waves are amplified and can be seen as concentrated dye lines. The dye line continues to be concentrated and the wave is amplified until a vortex line is formed. This discrete vortex line begins to take on some three-dimensional distortion and continues to roll up until a vortex loop is formed. The formation of a turbulent spot takes place near the tip of the vortex loop and eventual breakdown occurs. This transition process is essentially the same as observed in other cases. It is somewhat different, however, from that in the ordinary boundary layer over a flat plate as observed recently by Klebanoff. It is believed that, in the free-convection layer as in some other cases, the amplification rate is so high that the discrete vortices appear first before any other nonlinear mechanism begins to show up.

APPENDIX A

COMPUTATION OF THE INVISCID FUNCTION ϕ_1

The inviscid solution ϕ_1 is obtained, for a chosen combination of α and c, from the equation

$$(f'-c)(\phi''-\alpha^2\phi)-f'''\phi=0$$

with the boundary conditions

$$\phi(0)=0 \qquad\qquad \phi(\infty)=0 \quad .$$

For large values of η the derivatives of the velocity profile vanish and the equation reduces to

$$\phi''-\alpha^2\phi=0 \ .$$

The solutions are $\phi = e^{\pm\alpha\eta}$. Imposing the condition $\phi(\infty)=0$, we see that only $\phi = e^{-\alpha\eta}$ is acceptable. Thus the exponential solution gives the necessary starting values to numerically integrate from infinity inward to the wall. A difference scheme was used and integration of the equation

$$\phi''-\left(\alpha^2-\frac{f'''}{f'-c}\right)\phi=0$$

was continued until the neighborhood of the singular point ($f' = c$) was reached. In this neighborhood the solutions are given by equations (37) and (38). These two series solutions are matched to the value and the slope of ϕ obtained from the numerical integration procedure.

Once the series solutions take us through the singular point,

numerical integration is again started. This integration is continued until the solution comes into the neighborhood of the second singular point. Here the series solutions given by equations (39) and (40) are matched and the numerical integration is continued to the wall where $\phi(0)$ and $\phi'(0)$ are obtained. Thus the inviscid part of the eigenvalue problem is calculated for a given combination of α and c.

APPENDIX B

ASYMPTOTIC SERIES EXPANSIONS FOR THE TIETJENS FUNCTION AS GIVEN BY MILES [32]

Using Miles" notation we have:

$$\mathcal{F}(z) = \left[1 - F(z)\right]^{-1} = -z \int_{\infty}^{-z} f_3(s)\,ds \Big/ \int_{\infty}^{-z} s f_3(s)\,ds$$

where

$$f_3(s) = s^{\frac{1}{2}} H^{(1)}_{\frac{1}{3}}\left[\frac{2}{3}(is)^{\frac{3}{2}}\right] ,$$

$$\mathcal{F}(z) \sim 1 + \frac{e^{i\pi/4}}{z^{3/2}} + \frac{9}{4}\,\frac{e^{i\pi/2}}{z^{3}} + \frac{263}{32}\,\frac{e^{3i\pi/4}}{z^{9/2}} + O(z^{-6}) .$$

$$\sim 1 + \frac{e^{-5i\pi/4}}{s^{3/2}} + \frac{9}{4}\,\frac{e^{-i\pi/2}}{s^{3}} + \frac{263}{32}\,\frac{e^{i\pi/4}}{s^{9/2}} + O(s^{-6}) .$$

For large z, say $z > 10$, this asymptotic expansion is quite adequate and the second expansion $s = -z > 5$ gives the accuracy better than 0.1%.

SELECTED BIBLIOGRAPHY

1. Schubauer, G. B. and Skramstad, H. K., "Laminar Boundary-Layer Oscillations and Transition on a Flat Plate", J. Research Natl. Bur. Standards, Vol. 38, 1947, p. 251.

2. Schubauer, G. B. and Klebanoff, P. S., "Contributions on the Mechanics of Boundary-Layer Transition", NACA Rep. 1289, 1956, (Supersedes NACA TN 3489, 1955).

3. Klebanoff, P. S. and Tidstrom, K. D., "Evolution of Amplified Waves Leading to Transition in a Boundary-Layer with Zero Pressure Gradient", NASA TN D-195, 1959.

4. Schubauer, G. B., "Mechanism of Transition at Subsonic Speeds", Boundary Layer Research Symposium, Freiburg 1957, Edited by H. Goertler (Springer, Berlin, Germany, 1958), p. 85.

5. Hama, F. R., Long, J. D., and Hegarty, J. C., "On Transition from Laminar to Turbulent Flow", Inst. Fluid Dyn. Appl. Math., Univ. of Md., TN BN-81, 1956, also J. Appl. Phys. Vol. 28, p. 388, 1957.

6. Hama, F. R., "Boundary-Layer Transition Induced by a Vibrating Ribbon on a Flat Plate", Inst. Fluid Dyn. Appl. Math., Univ. of Md., TN BN-195, 1960, also Proceedings of the 1960 Heat Transfer and Fluid Mechanics Institute, Stanford Univ., p. 92.

7. Fales, E. N., A New Laboratory Technique for Investigation of the Origin of Fluid Turbulence, J. Franklin Inst., Vol. 259, p. 491, 1955.

8. Hama, F. R., "Note on the Boundary-Layer Instability on a Flat Plate Stopped Suddenly", J. Aero. Sci., Vol. 24, p. 471, 1957.

9. Hegarty, J. C., "Investigation of Transition Caused by the Stopping of a Flat Plate", Univ. of Md., Inst. Fluid Dyn. Appl. Math., TN BN-141, 1958.

10. Hama, F. R., (See Reference 5)

11. Hama, F. R., "Three-Dimensional Vortex Pattern Behind a Circular Cylinder, J. Aero. Sci., Vol. 24, p. 156, 1957.

12. Eckert, E.R.G., and Soehnghen, E., "Interferometric Studies on the Stability and Transition to Turbulence of a Free-Convection Boundary Layer", Proceedings of the General Discussion on Heat Transfer; London, England, p. 321, 1951.

13. Birch, W. D., "On the Stability of Free-Convection Boundary Layers on a Vertical Flat Plate", M. S. Thesis, Air Force Inst. of Tech., Air Univ., 1957.

14. Gartrell, H. E., "On the Oscillations of Free-Convection Boundary Layers", Masters Thesis, Air Univ., 1959.

15. Saunders, O. A., "The Effect of Pressure Upon Natural Convection in Air", Proc. Roy. Soc., London, Series A, Vol. 157, p. 278, 1936.

16. Saunders, O. A., "Natural Convection in Liquids", Proc. Roy. Soc., London, Series A, Vol. 172, p. 55, 1939.

17. Hermann, R., "Heat Transfer by Free-Convection from Horizontal Cylinders in Diatomic Gases", NACA TM 1366, 1936.

18. Fujii, T., "On the Development of a Vortex Street In a Free-Convection Boundary Layer", Japan Soc. Mech. Engrs., Vol. 2, No. 8, p. 551, 1959.

19. Larson, J. R., "Boundary-Layer Transition in Natural Convection", M. S. Thesis, Univ. of Wash., 1960.

20. Plapp, J. E., "Laminar Boundary-Layer Stability in Free Convection" Pt. 1, Ph. D. Thesis, Cal. Inst. of Tech., 1957. See also Jour. of Aero. Sc., Vol. 24, p. 318, 1957.

21. Pohlhausen, E., "Der Wärmeaustausch zwischen festen Körpern und Flüssigkeiten mit kleiner Reibung und kleiner Wärmeleitung" ZAMM, Vol. 1, p. 115, 1921.

22. Schuh, H., "Einige Probleme bei freier Strömung zäher Flüssigkeiten" (1946, unpublished) see also Göttinger Monographien 1946, Vol. B, Grenzschichten.

23. Ostrach, S., "An Analysis of Laminar Free-Convection Flow and Heat Transfer About a Flat Plate Parallel to the Direction of the Generating Body-Force", NACA TN 2635, 1952 (superseded by Rep. 1111, 1953).

24. Squires, H. B., "On the Stability for Three-Dimensional Disturbances of Fiscous Fluid Flow Between Parallel Walls", Proc. of Roy. Soc., Vol. 142, Series A, p. 621, 1933.

25. Ostrach, S., Chap. 6 "Hydrodynamic Stability" of a Princeton Series Book to be published.

26. Lin, C. C., The Theory of Hydrodynamic Stability , Cambridge Univ. Press, 1955.

27. Tollmien, W., "The Production of Turbulence", NACA TM 609, 1931.

28. Tietjens, O., "Beitrage zur Entstehung der Turbulenz" Z. angew. Math. Mech., Vol. 5, p. 200, 1925.

29. Squire, H. B., Heat Transfer, Vol. 2, Chap. 14 of Modern Developments in Fluid Dynamics, High Speed Flow , Howarth, L. (ed.) Claredon Press, Oxford, 1953.

30. Gregory, N., Stuart, J. T., and Walker, W. S., "On the Stability of Three-Dimensional Boundary Layers with Application to the Flow Due to a Rotating Disk", Phil. Trans. of Roy. Soc. of London, Series A, No. 243, Vol. 248, p. 155, 1955.

31. Boltz, F. W., Kenyon, G. C., and Allen, C. Q., "Effects of Sweep Angle on the Boundary-Layer Stability Characteristics of an Untapered Wing at Low Speeds", NASA TN D-338, 1960.

32. Miles, J. W., "The Hydrodynamic Stability of a Thin Film of Liquid in Uniform Shearing Motion", J. Fl. Mech., Vol. 8, Part 4, 1960.

33. Foote, J. R., and Lin , C. C., "Some Recent Investigations in the Theory of Hydrodynamic Stability", Quart. App. Math., Vol. 8, p. 265, 1950.

34. Copson, E. T., An Introduction to the Theory of Functions of a Complex Variable, Oxford University Press, 1935.

35. Zaat, J. A., "Numenische Beiträge zur Stabilitatstheorie der Grenzschichten", Boundary Layer Research Symposium, Freiburg 1957, Edited by H. Goentlen (Springer, Berlin, Germany, 1958) p. 127.

TABLE 1

NEUTRAL DISTURBANCE EIGENVALUES FROM

CALCULATIONS BASED ON THE INNER-CRITICAL POINT

C	α	z_{i_0}	$G \times 10^{-5}$
0.0174	0.500	-2.66	9.73
0.0200	0.649	-2.74	5.50
0.0220	0.722	-2.86	4.27
0.0230	0.770	-2.87	3.53
0.0235	0.875	-3.03	3.47
0.0235	0.974	-3.25	3.70
0.0230	0.997	-3.32	4.28
0.0226	1.000	-3.36	4.64
0.0220	1.015	-3.46	5.36
0.0208	0.995	-3.60	7.29
0.0200	0.995	-3.66	8.56

TABLE 2

NEUTRAL DISTURBANCE EIGENVALUES FROM

CALCULATIONS BASED ON THE OUTER-CRITICAL POINT

C	α	z_{i_0}	G
0.005	1.6	16.5	5040
0.006	1.5	17.8	7212
0.007	1.37	19.4	8900
0.008	1.28	21.5	10,430

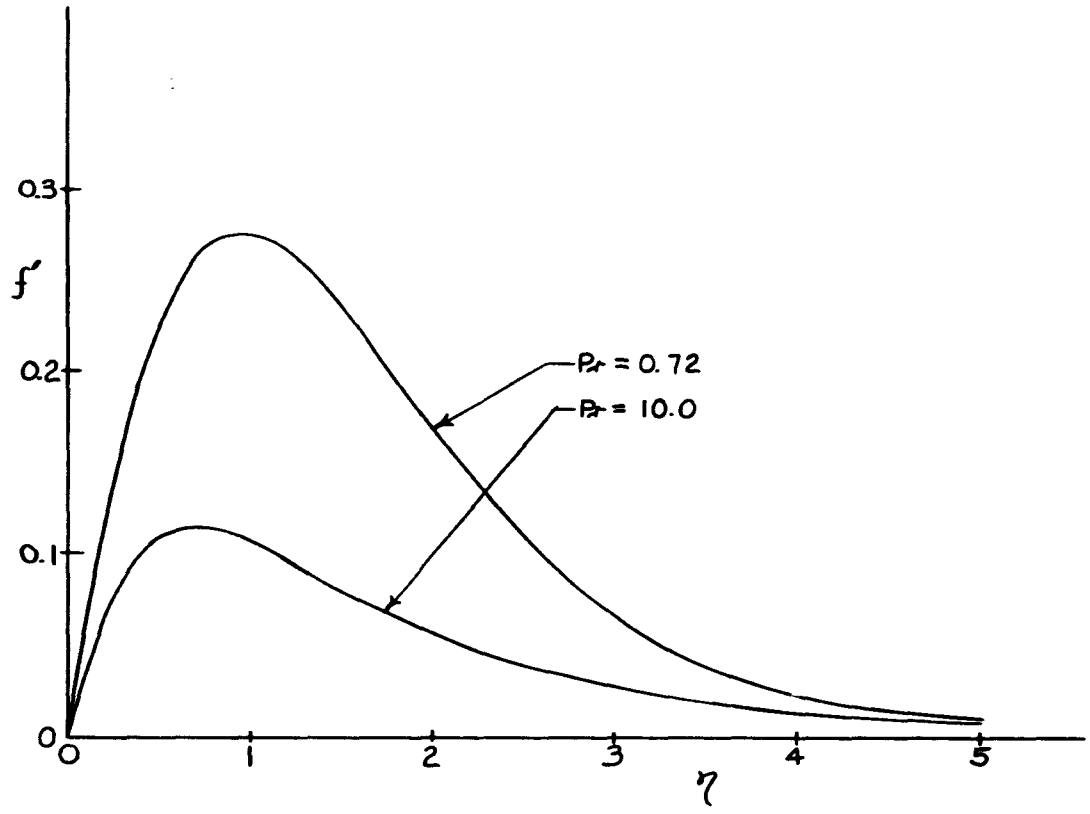

FIG.1 TYPICAL FREE-CONVECTION VELOCITY PROFILES

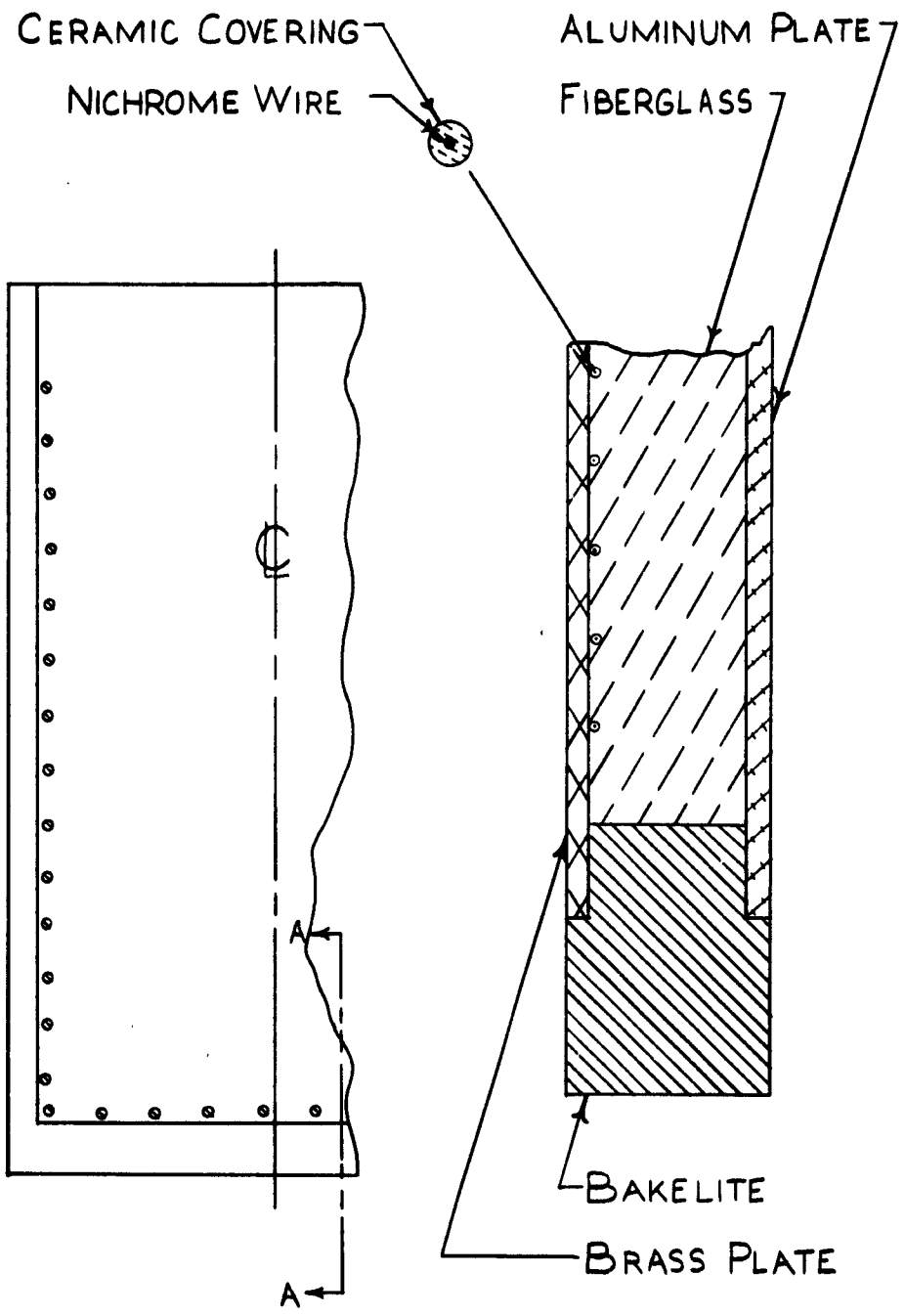

FIG 2. WALL CONSTRUCTION

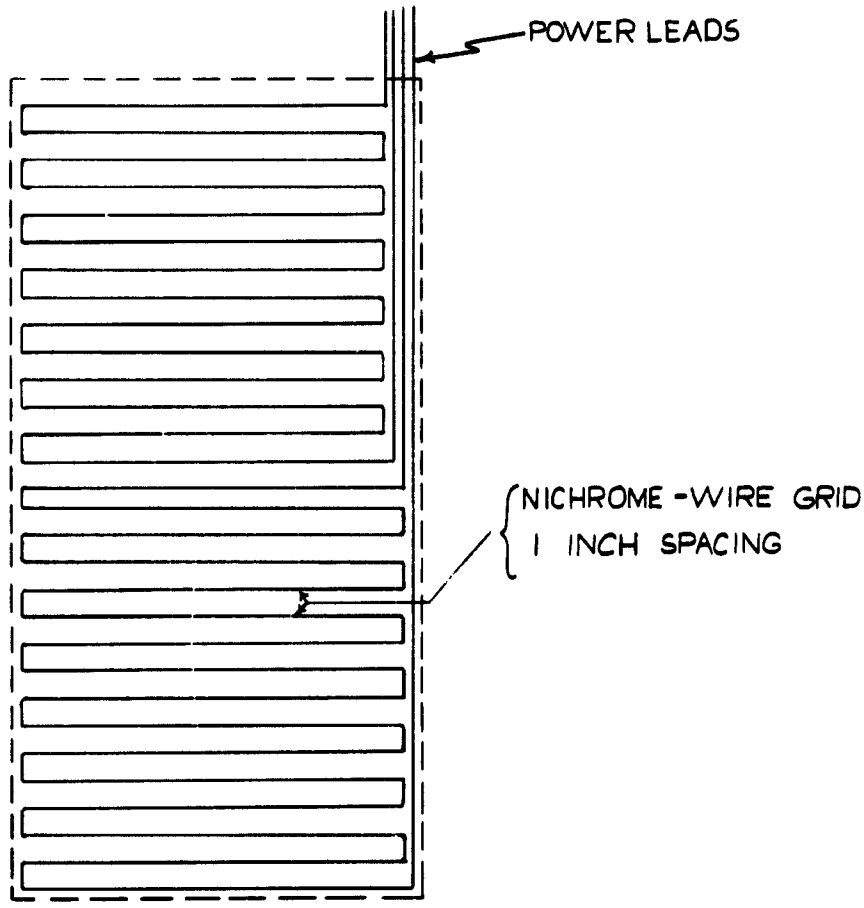

FIG. 3 SKETCH OF PARALLEL GRID CIRCUIT

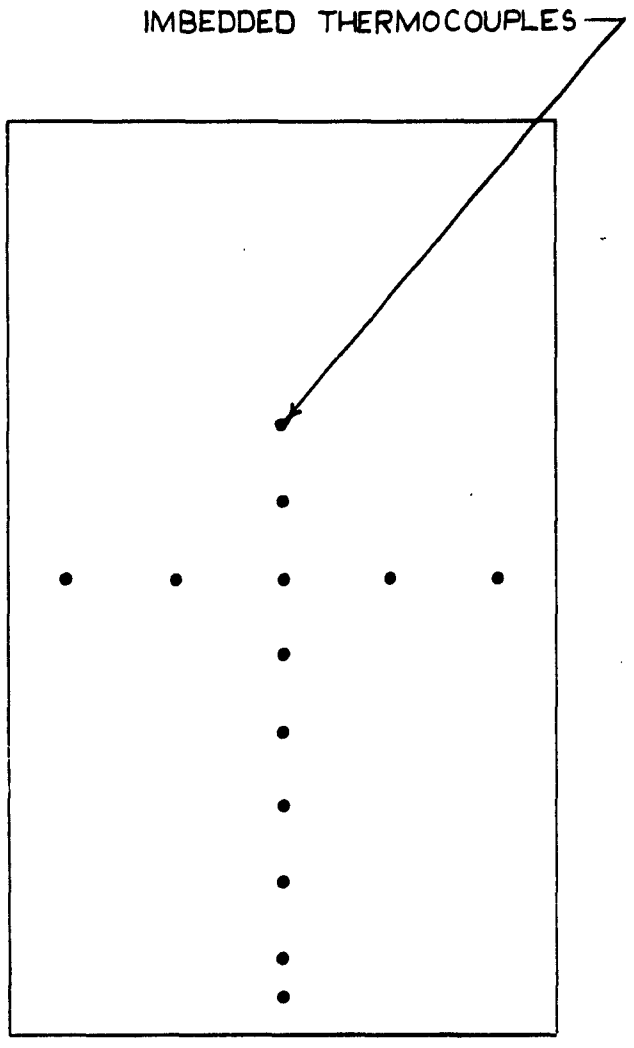

FIG. 4 IMBEDDED THERMOCOUPLE LOCATIONS

SCALE 1" = 1'

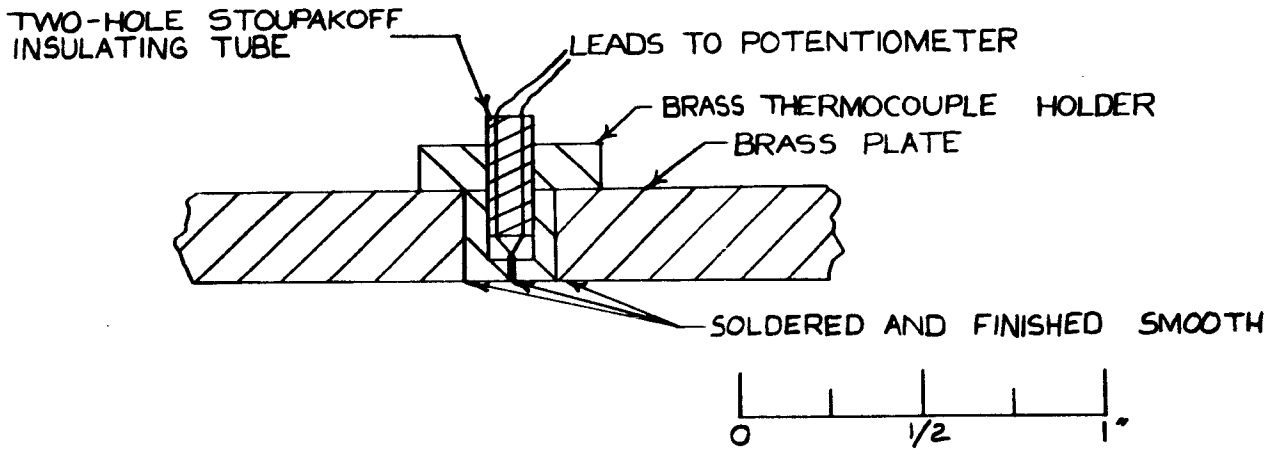

FIG. 5 DETAIL OF IMBEDDED THERMOCOUPLE

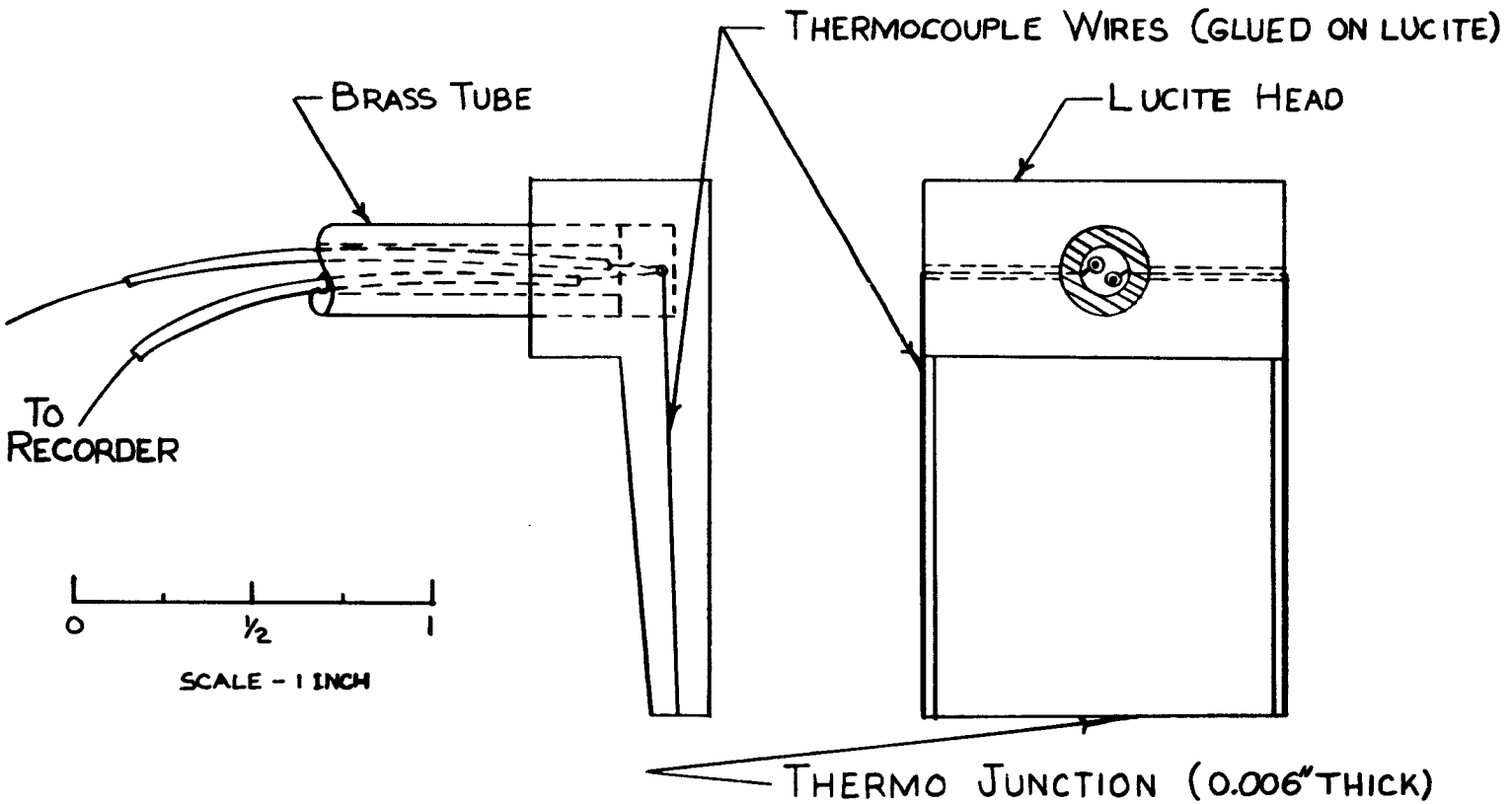

FIG 6 THERMOCOUPLE PROBE

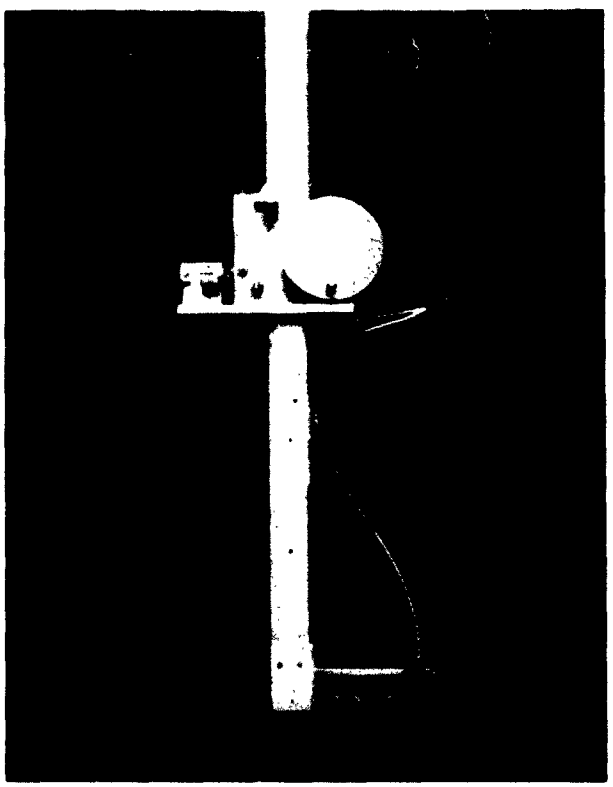

FIG. 7. TRAVERSING MECHANISM

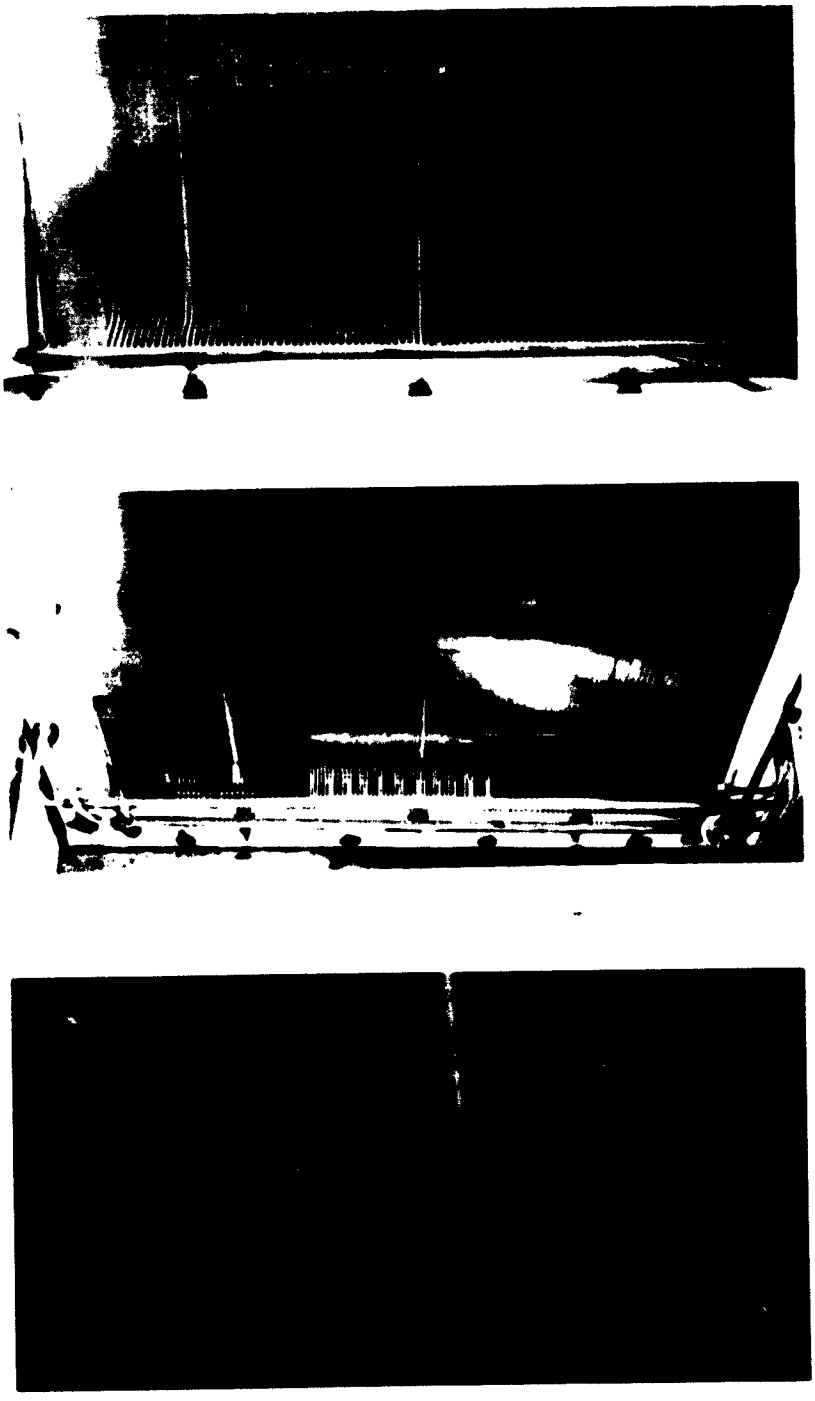

FIG.8 DYE RAKES AND DYE COMB

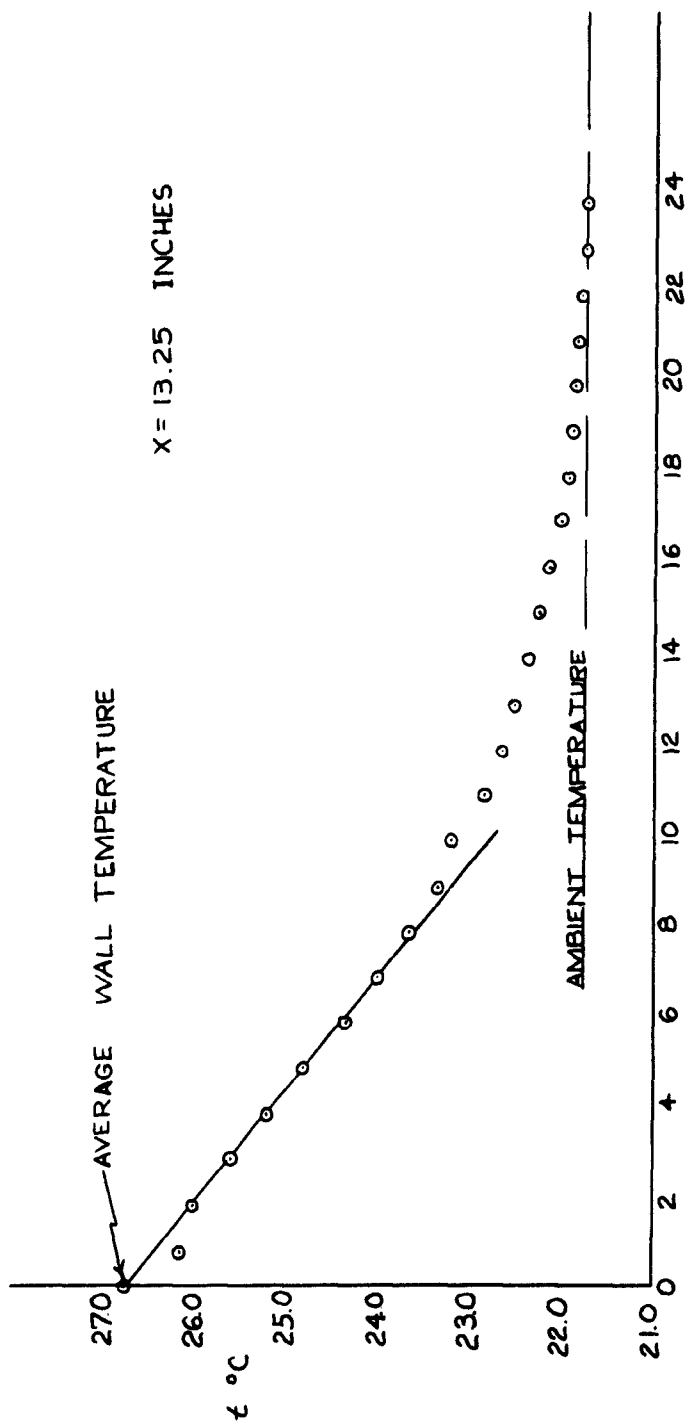

FIG.9 TYPICAL TEMPERATURE PROFILE

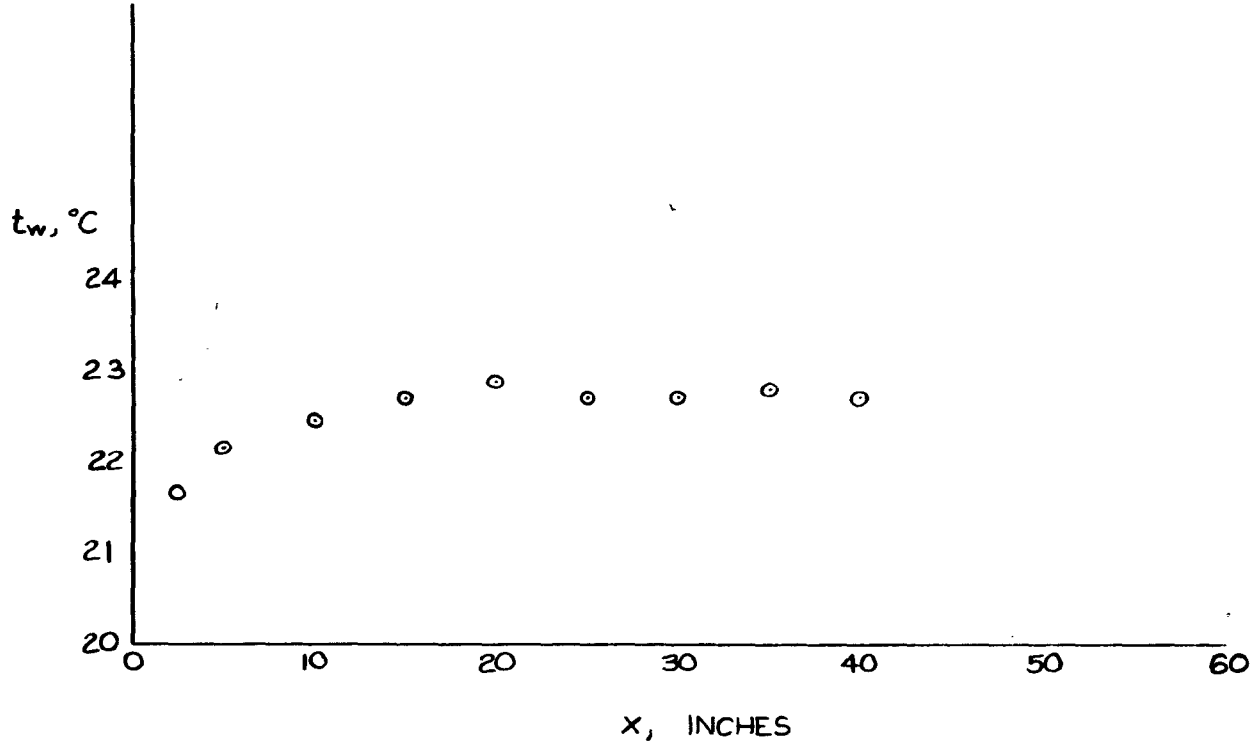

FIG.10 TYPICAL WALL TEMPERATURE DISTRIBUTION

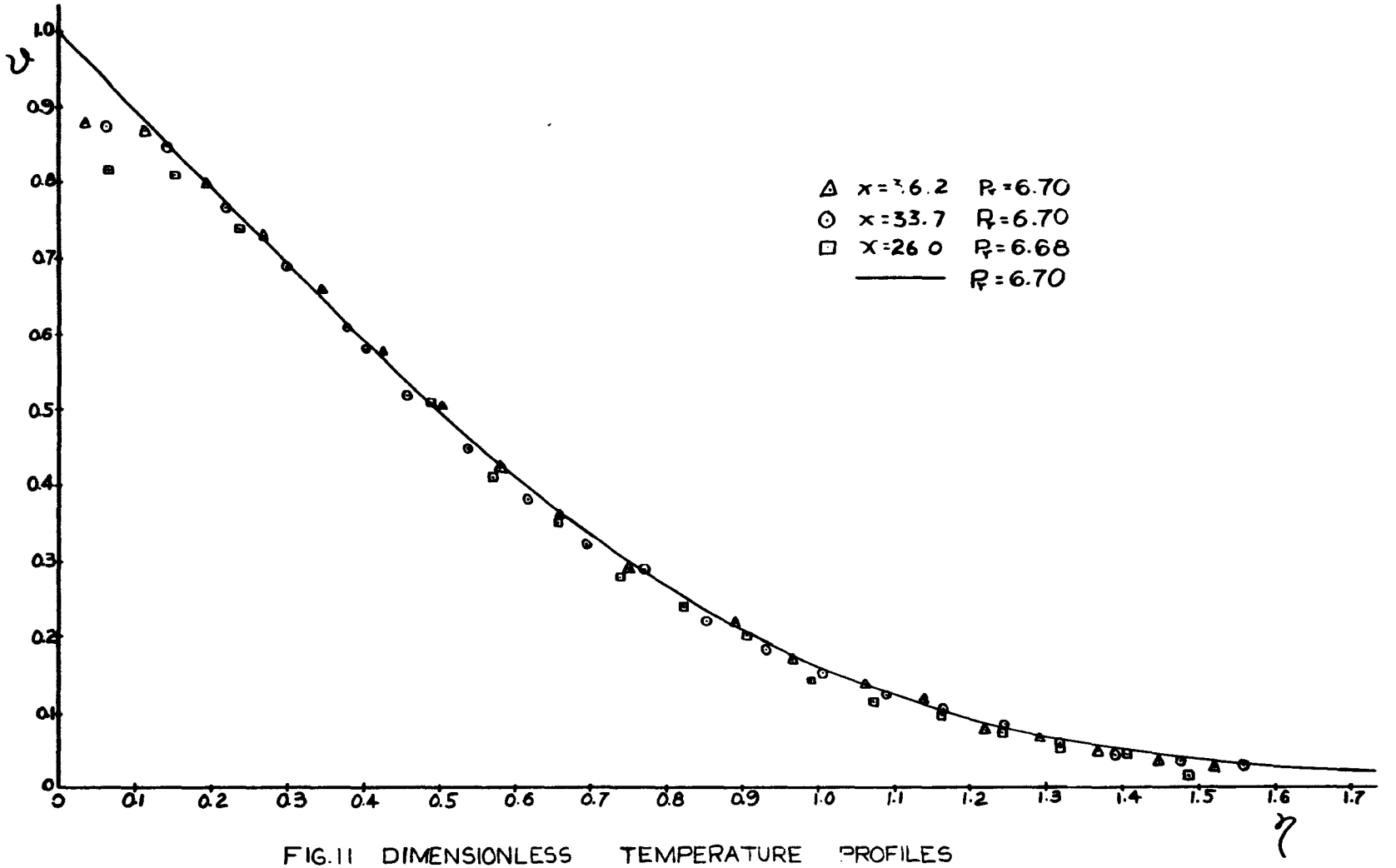

FIG. 11 DIMENSIONLESS TEMPERATURE PROFILES

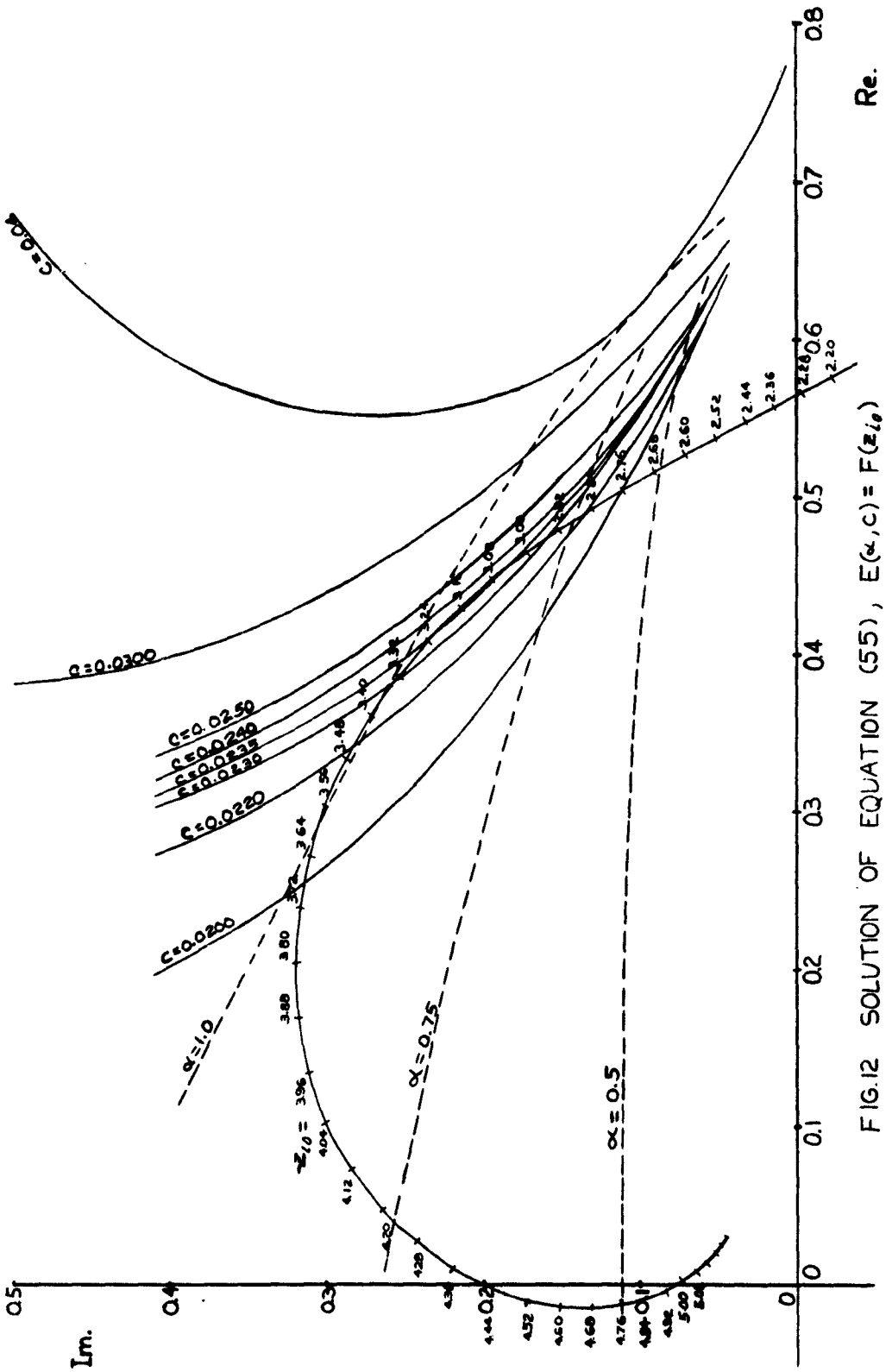

FIG.12 SOLUTION OF EQUATION (55), $E(\alpha, c) = F(z_{10})$

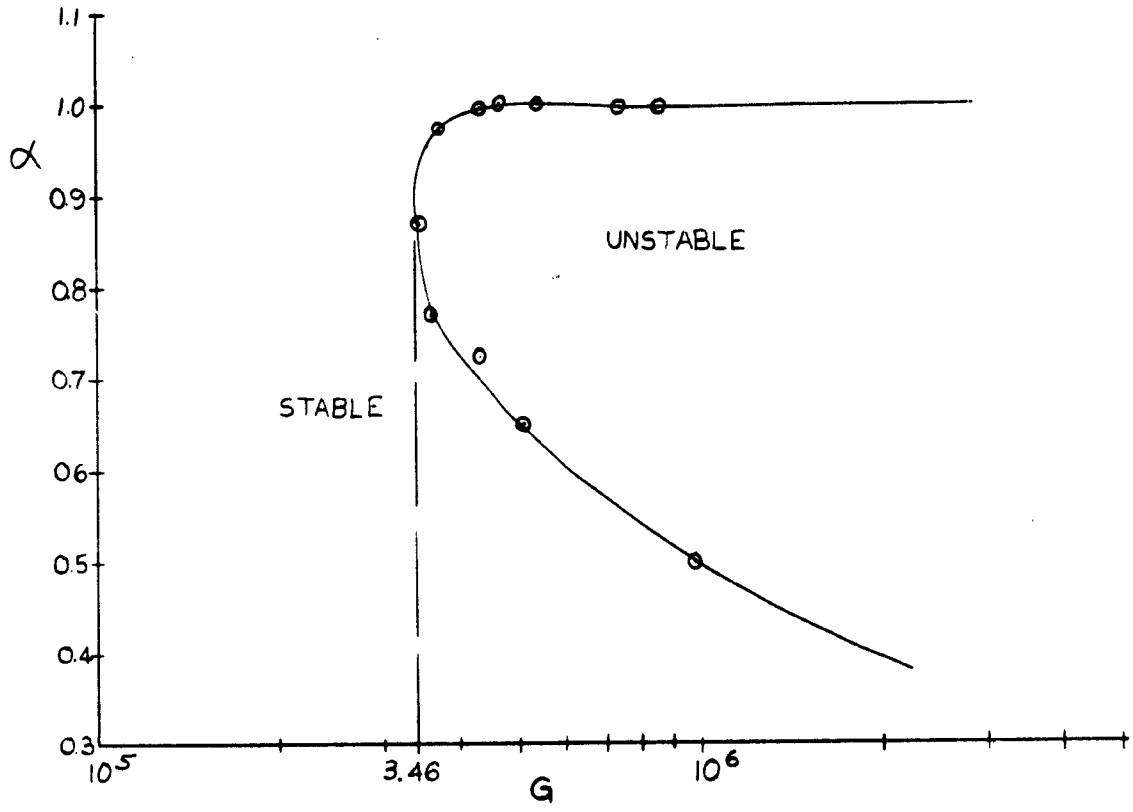

FIG. 13 INDIFFERENCE CURVE FOR THE WAVE LENGTH FROM CALCULATIONS BASED ON THE INNER CRITICAL POINT

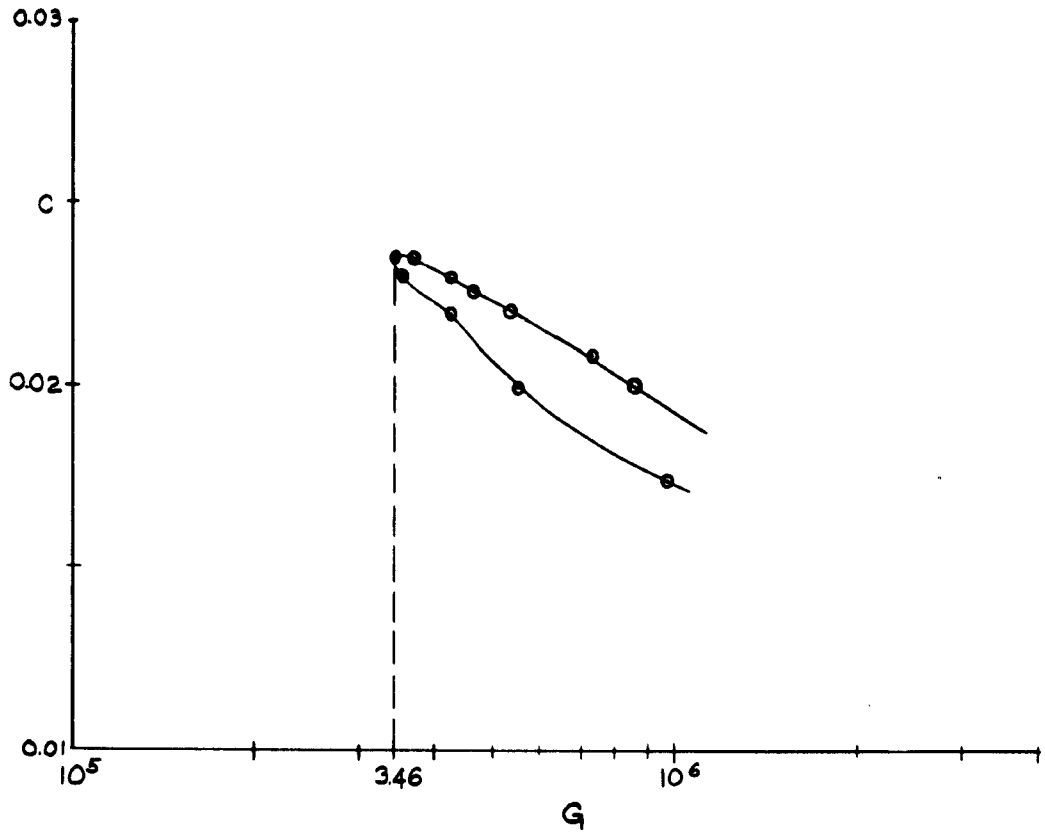

FIG. 14 INDIFFERANCE CURVE FOR THE VELOCITY OF WAVE PROPAGATION

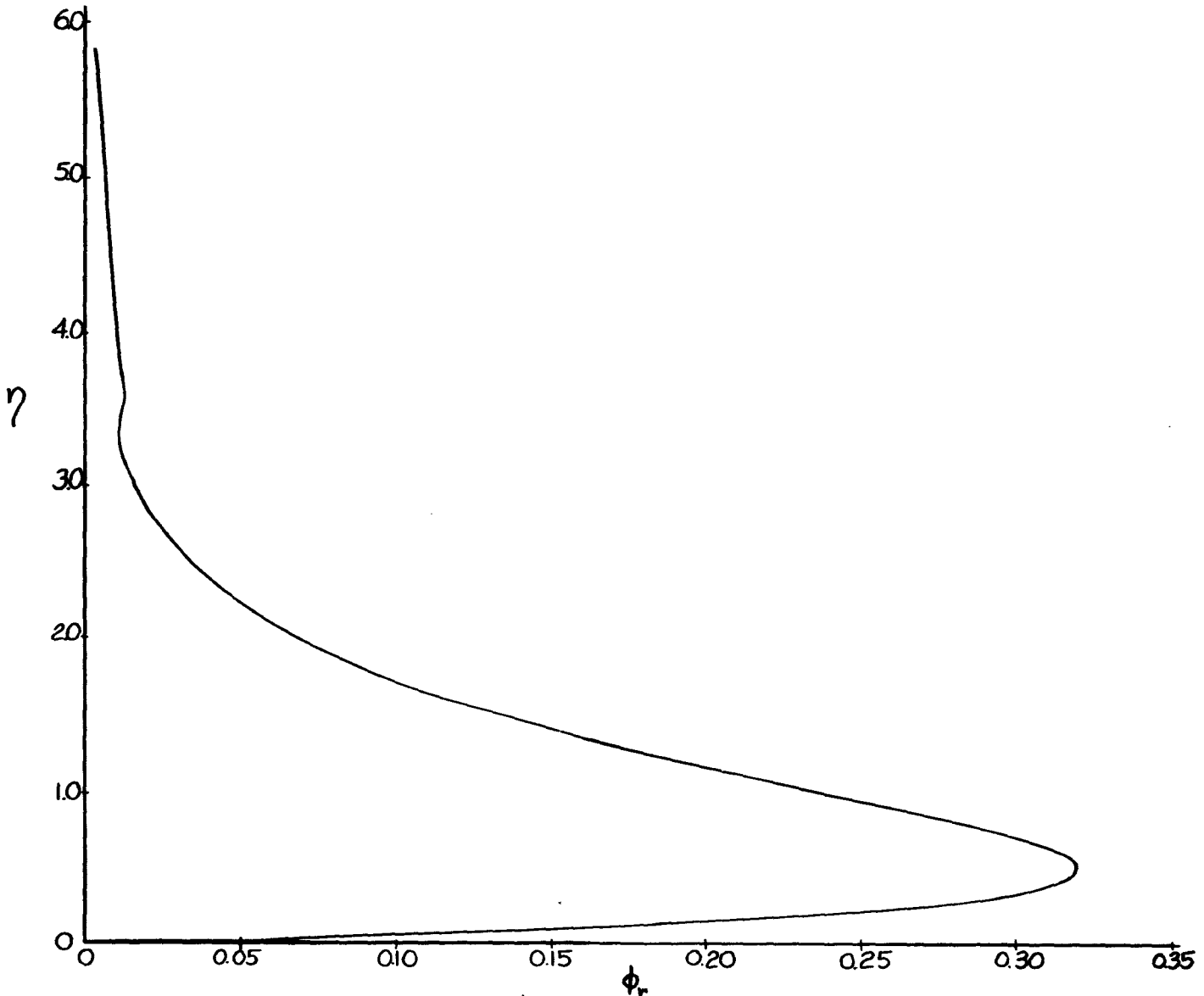

FIG. 15 INVISCID FUNCTION ϕ_1 FOR A NEUTRAL OSCILLATION

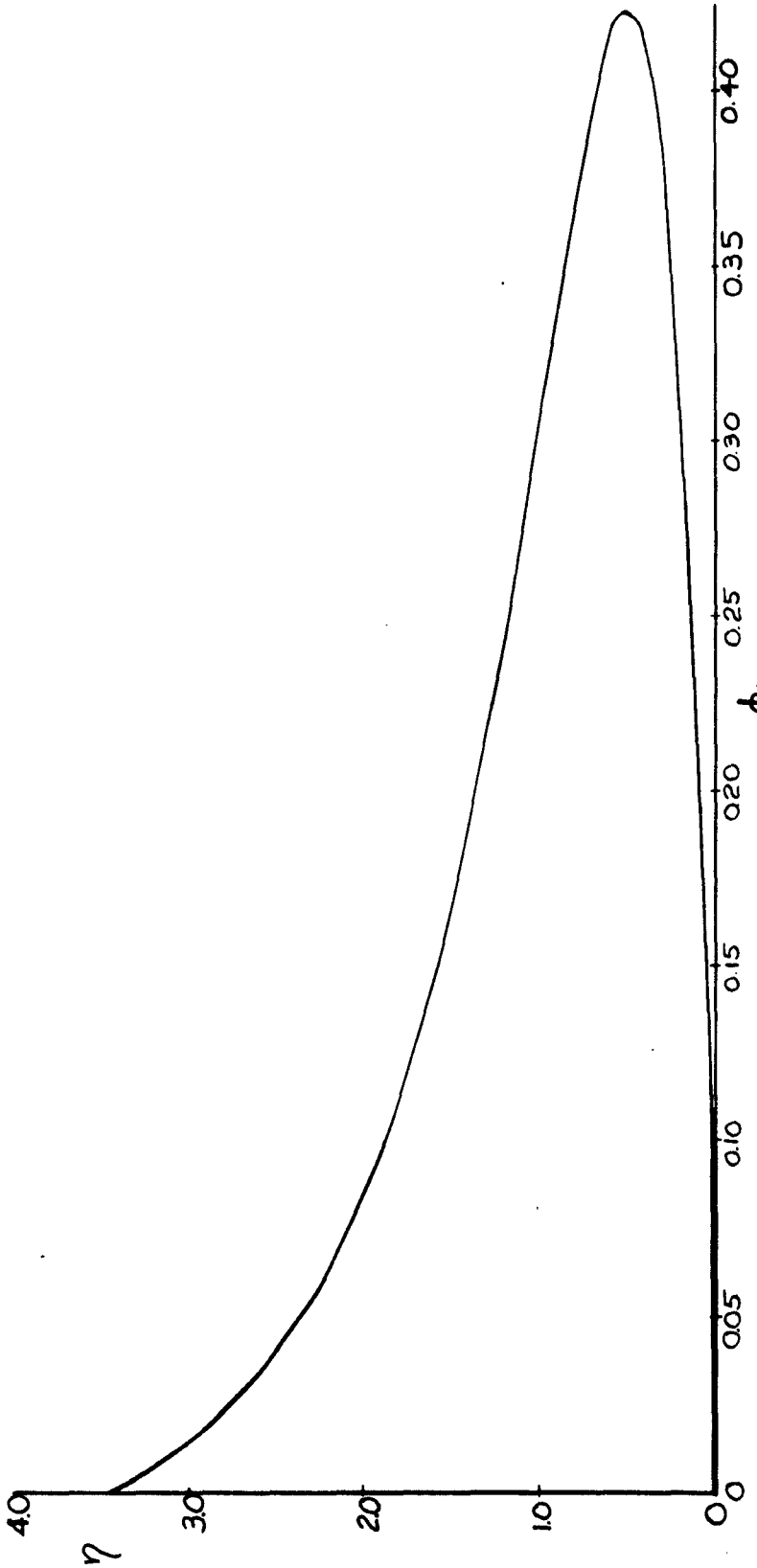

FIG. 15 CONTINUED

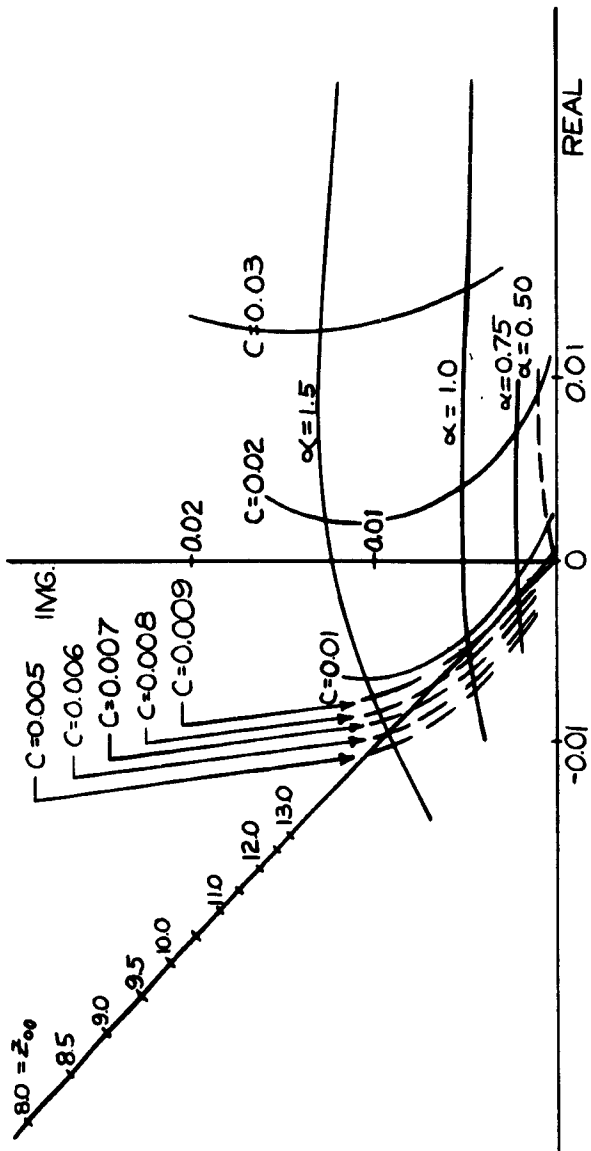

FIG. 16 SOLUTION OF EQUATION (58), $\mathcal{E}(\alpha, C) = \mathcal{F}(z_0)$

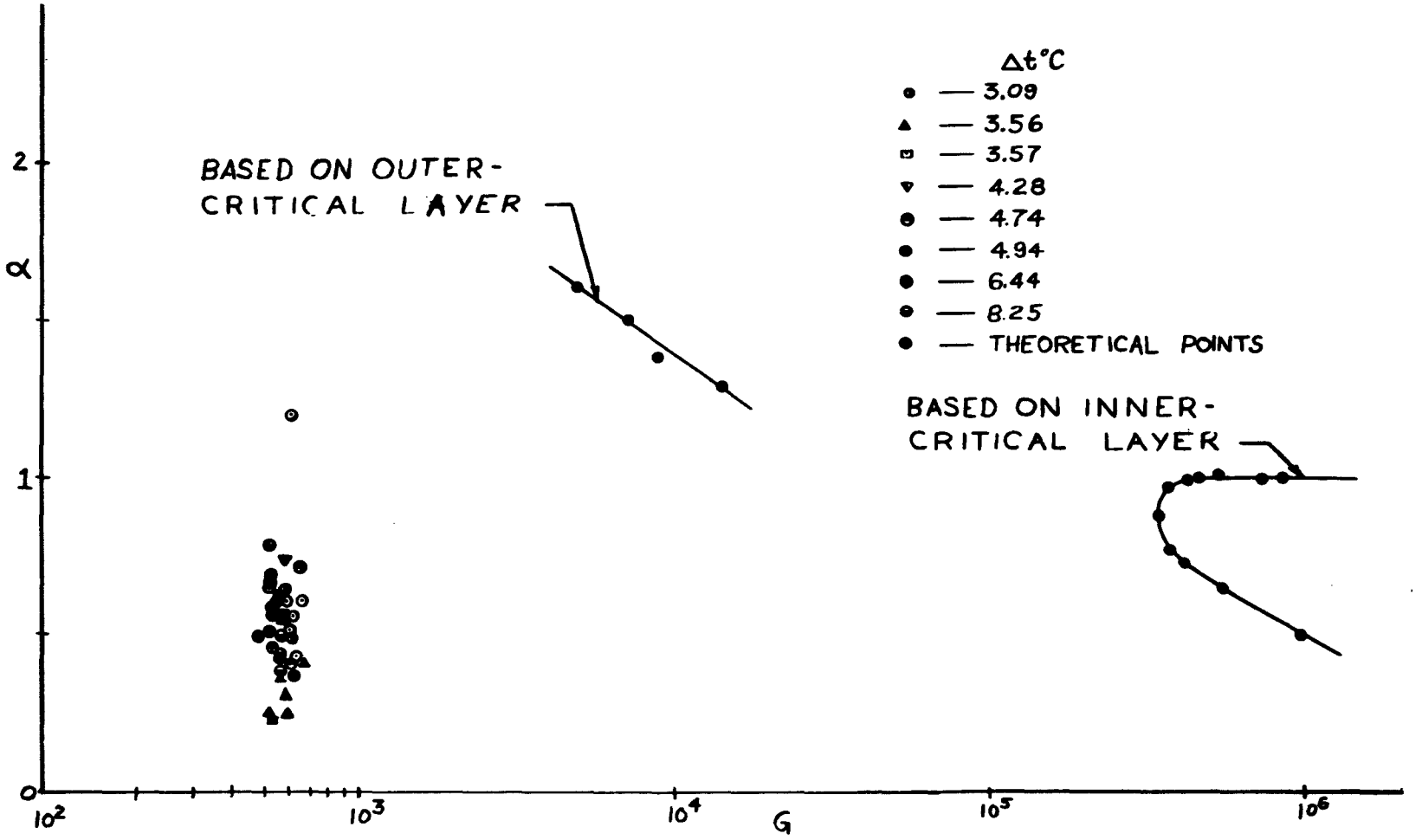

FIG. 17 INDIFFERNCE CURVES FOR THE WAVE LENGTH FROM CALCULATIONS BASED ON THE INNER- AND OUTER-CRITICAL POINTS ALONG WITH THE EXPERIMENTAL DATA OBTAINED FROM INNER-CRITICAL LAYER

G = 478 α = 0.493

G = 520 α = 0.509

FIG. 19 PLAN VIEW OF VORTEX DEVELOPMENT AT ΔT = 6.44 °C

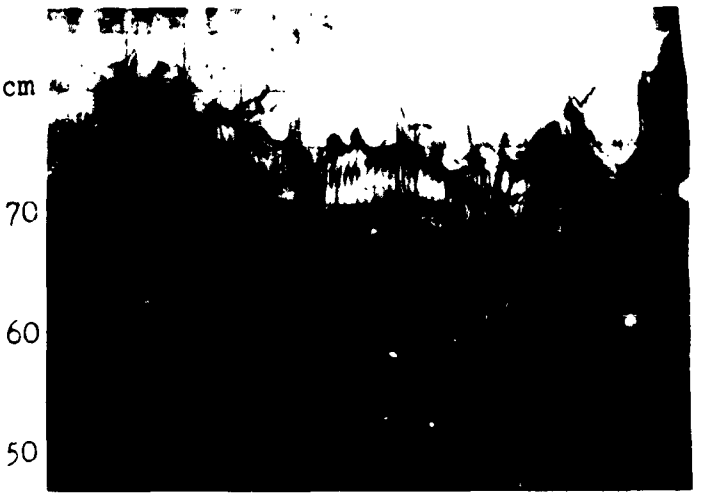

G = 667 α = 0.521

G = 621 α = 0.453

FIG. 20 PLAN VIEW OF VORTEX DEVELOPMENT AT $\Delta T = 3.57°C$

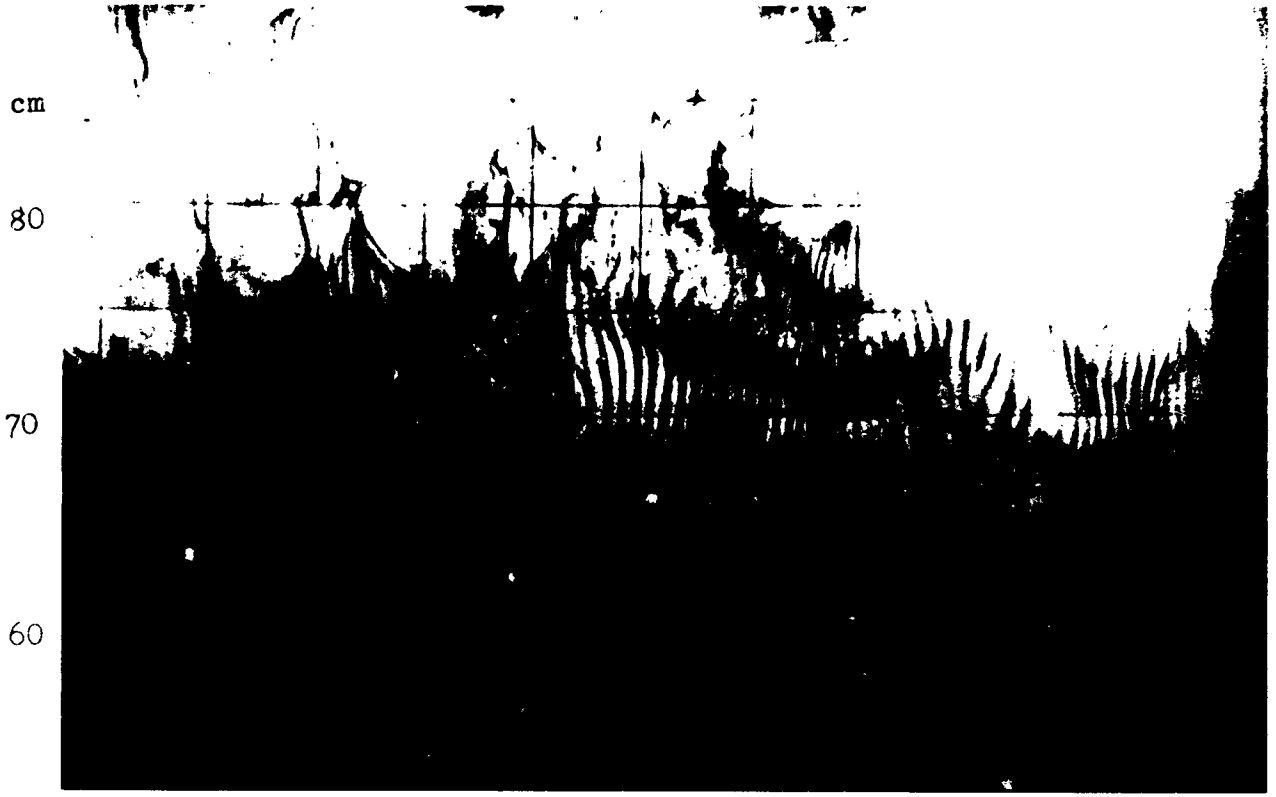

G = 577 α = 0.468

FIG. 21 PLAN VIEW OF VORTEX DEVELOPMENT

AT $\Delta T = 3.56^{\circ} C$

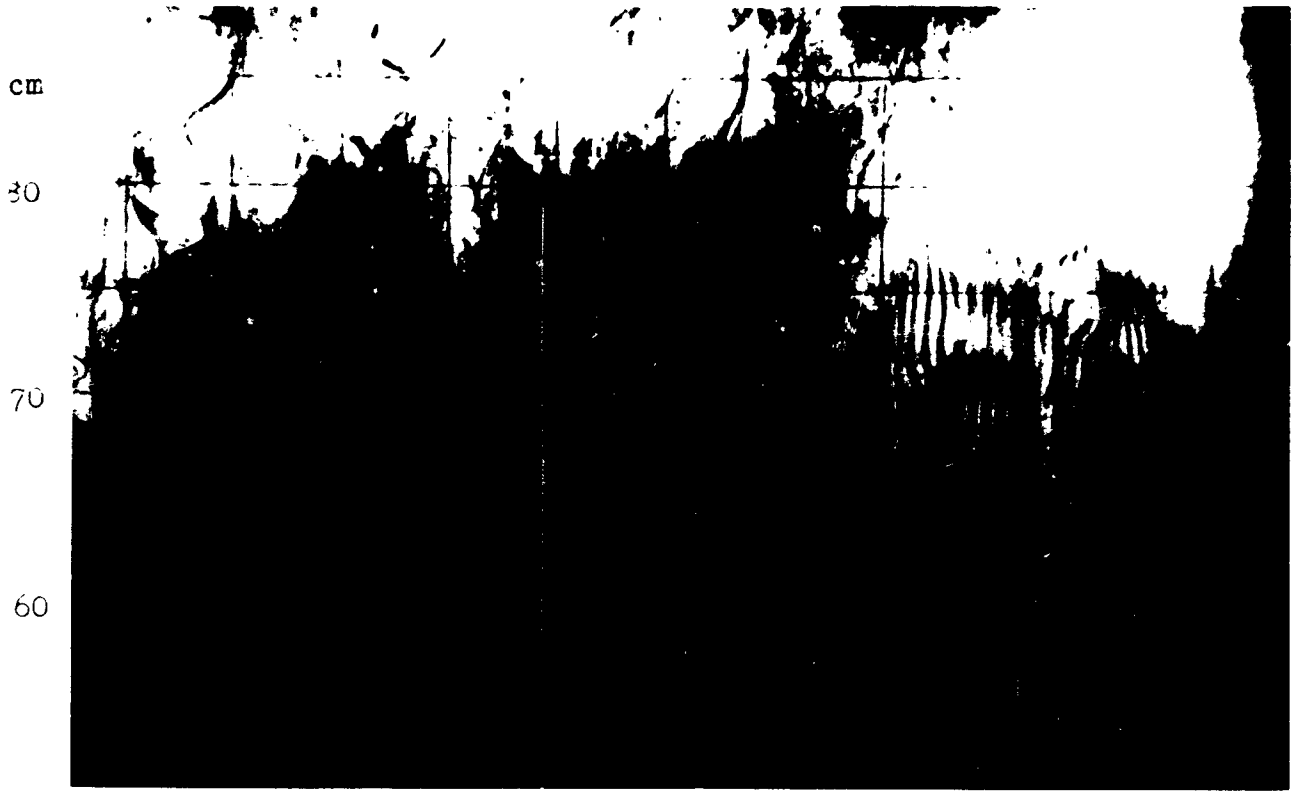

G = 590 α = 0.510

FIG. 22 PLAN VIEW OF VORTEX DEVELOPMENT

AT $\Delta T = 3.56\,^{\circ}C$

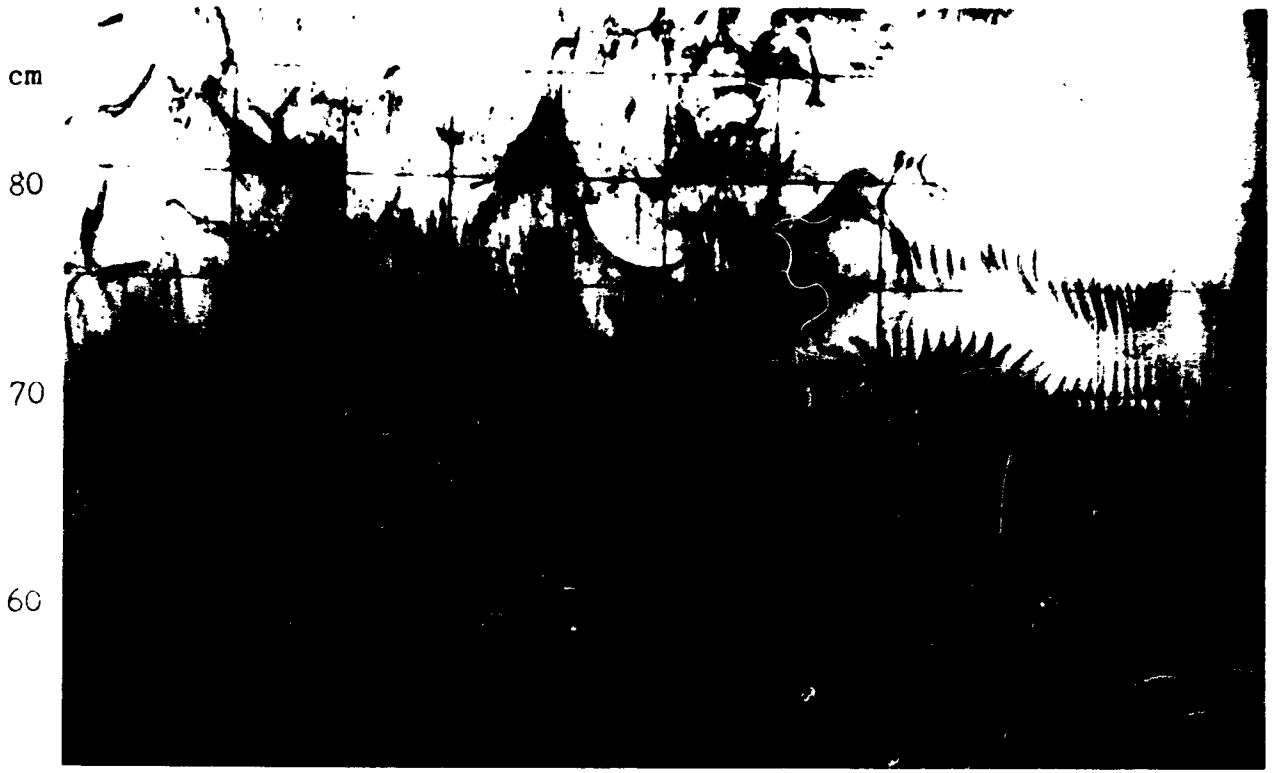

G = 574 α = 0.512

FIG. 23 PLAN VIEW OF VORTEX DEVELOPMENT AT $\Delta T = 4.28\,^{\circ}C$

G = 580 α = 0.742

FIG. 24 PLAN VIEW OF VORTEX DEVELOPMENT AT $\Delta T = 4.28^{\circ} C$

a) y = 0

b) y = 0.030 inch

c) y = 0.060 inch

FIG. 25 PLAN AND SIDE VIEWS OF A SINGLE DYE STREAK PATTERN AT $\Delta T = 7.20^{\circ} C$

d) y = 0.090 inch

e) y = 0.120 inch

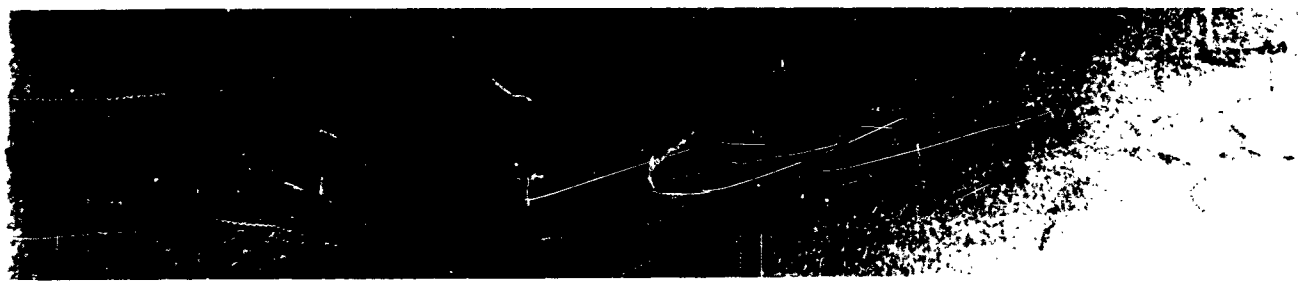

f) y = 0.150 inch

FIG. 25 CONTINUED

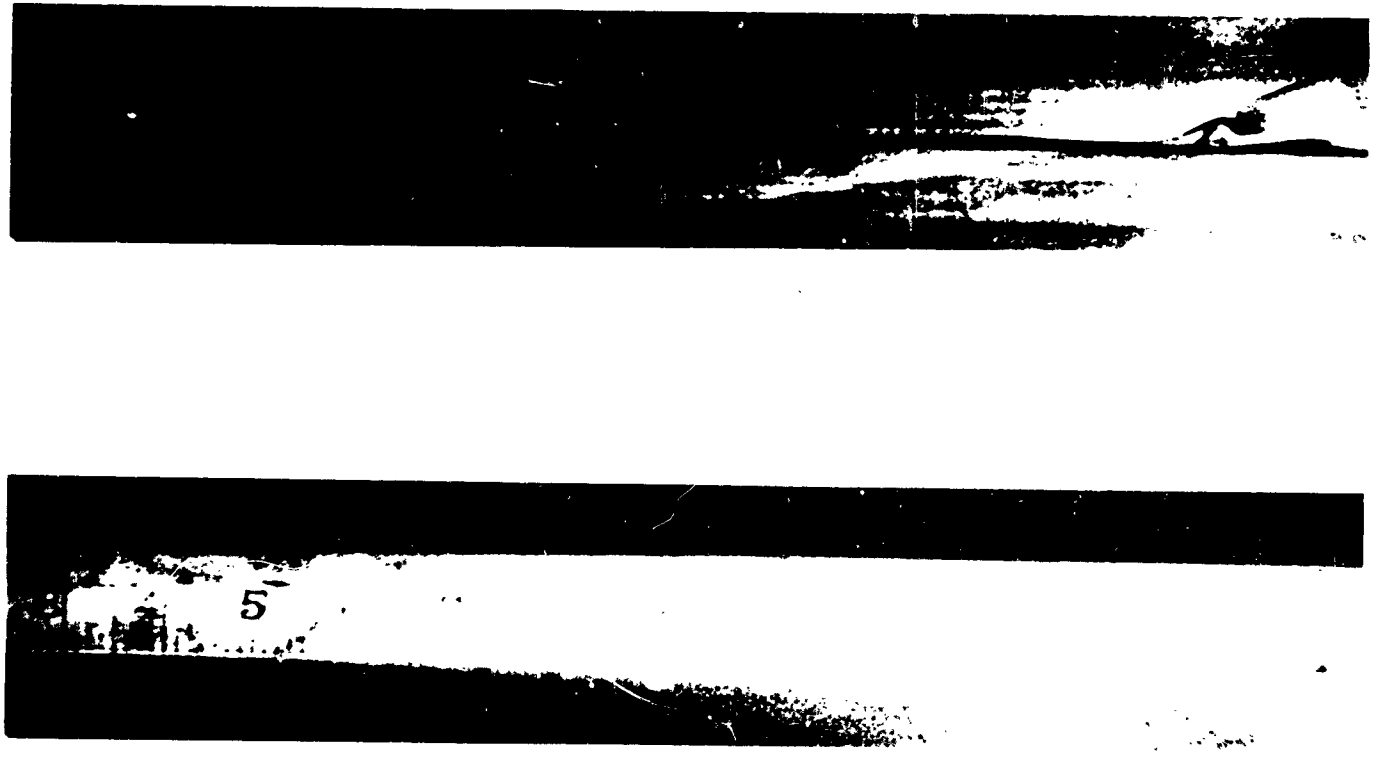

FIG. 25 CONTINUED

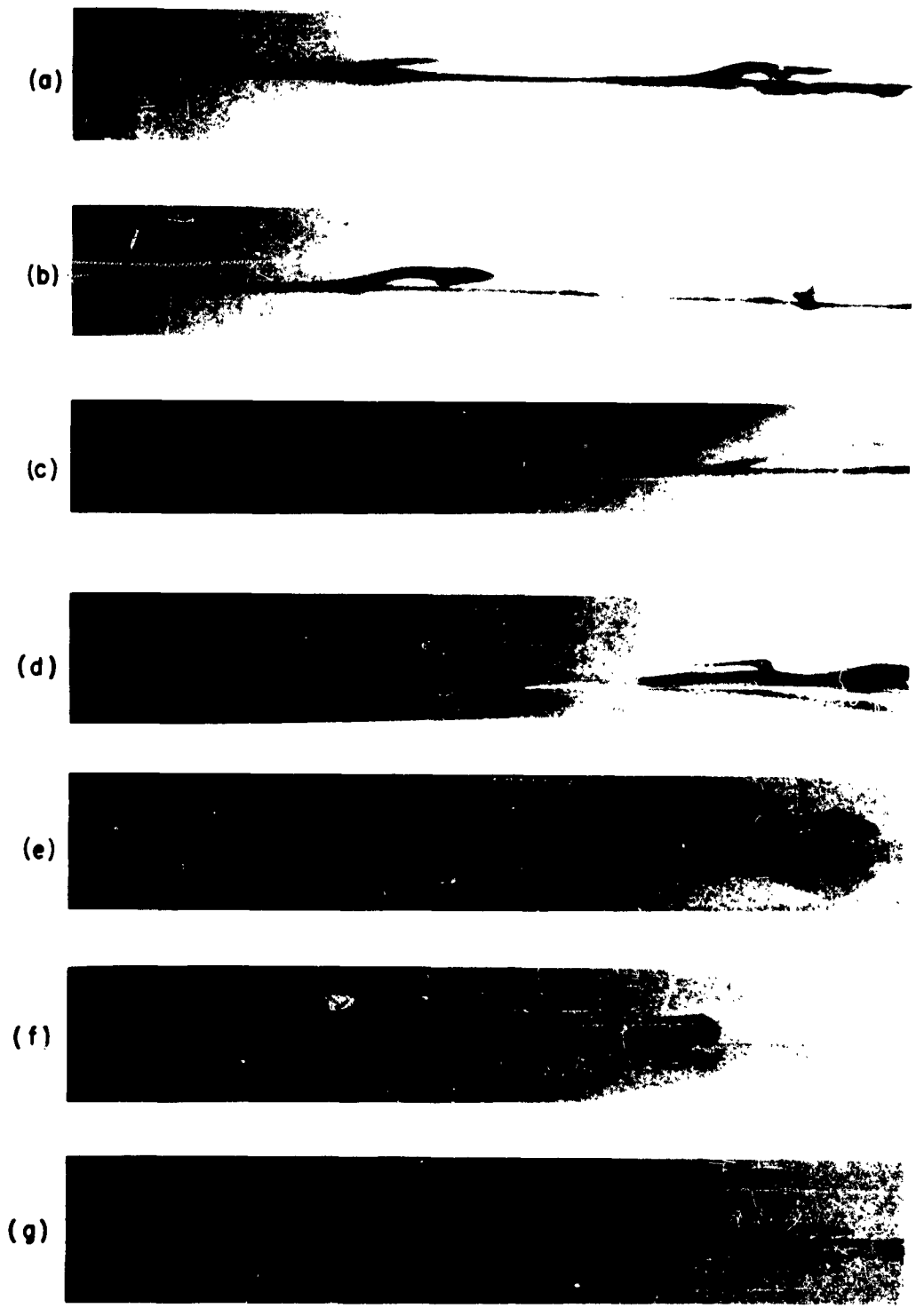

FIG. 26 SIDE VIEWS OF A SINGLE DYE STREAK AT $\Delta T = 5.20^{\circ}C$

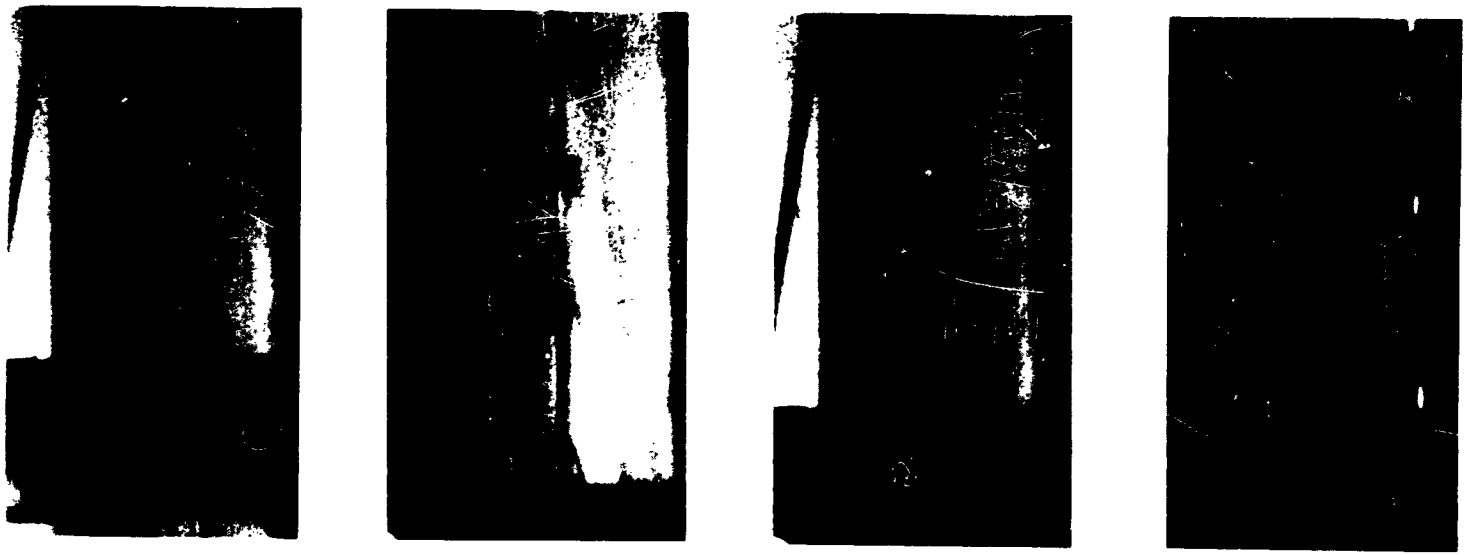

FIG. 27 SIDE VIEW OF VORTEX DEVELOPMENT OBSERVED FROM TWO DYE STREAKS

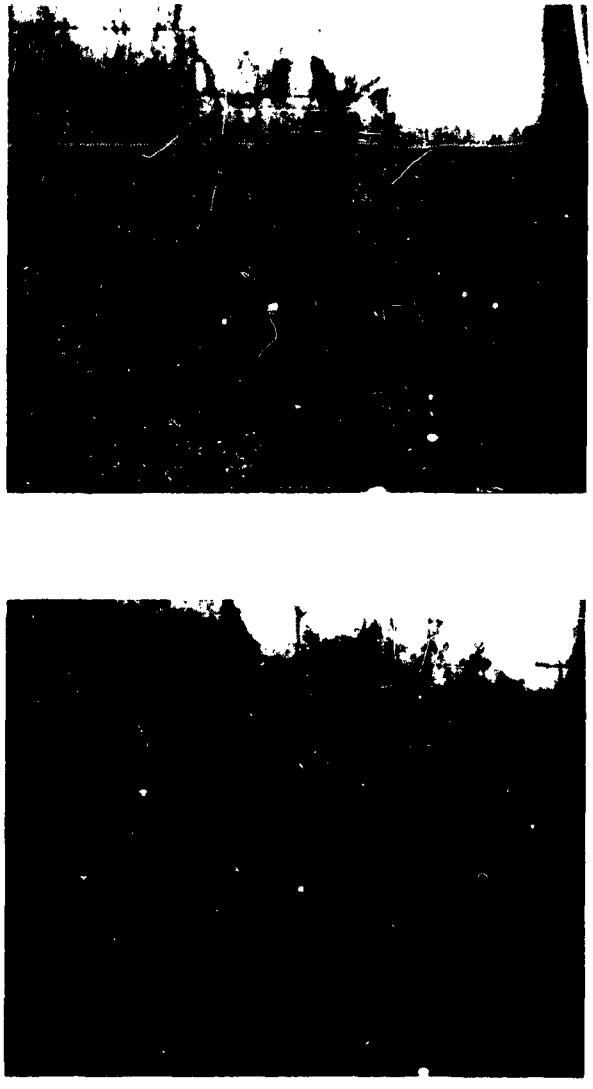

FIG. 28 PLAN VIEWS OF VORTEX DEVELOPMENT AT $\Delta T = 6.00\,^{\circ}C$

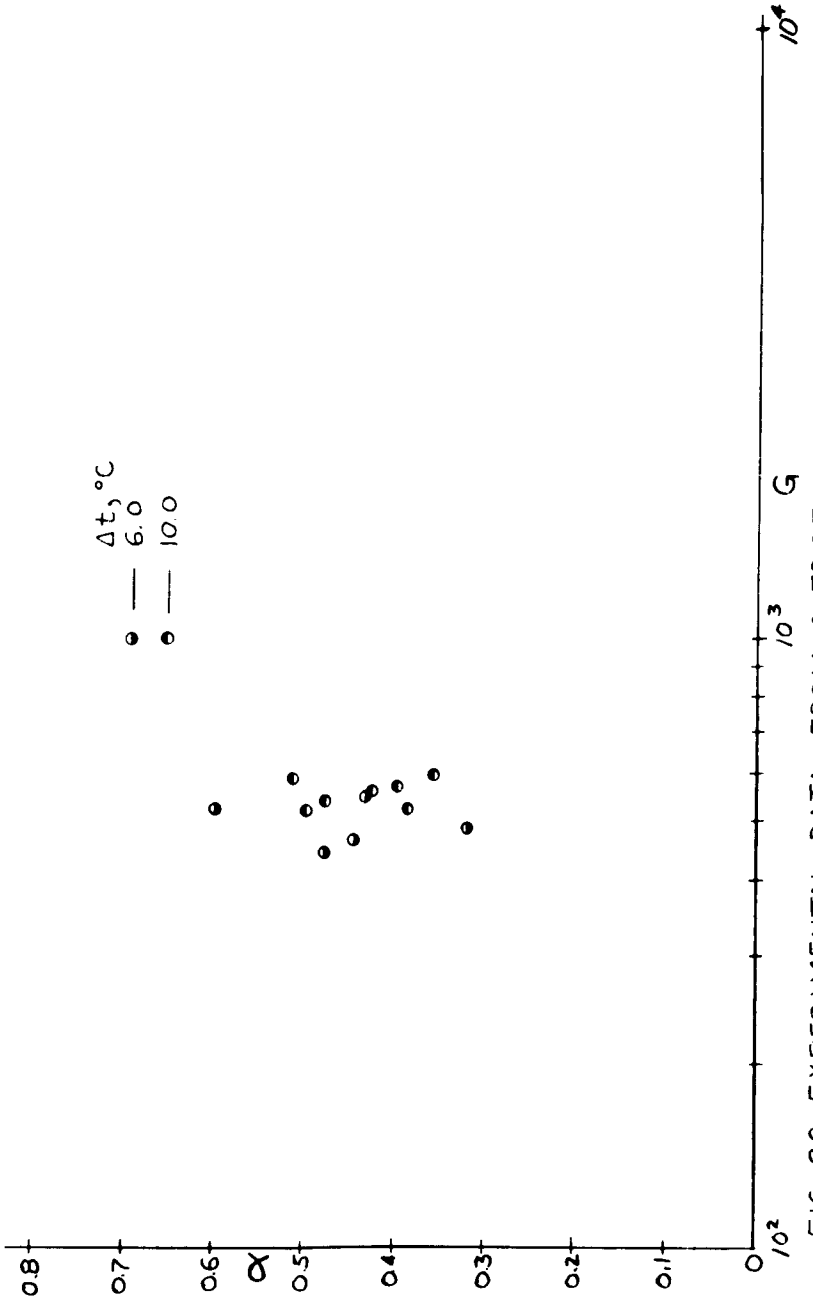

FIG. 29 EXPERIMENTAL DATA FROM OUTSIDE DISTURBANCE WAVE